Non-Orthogonal Multiple Access (NOMA) in Uplink Poisson Cellular Networks With Power Control

Yanan Liang, *Student Member, IEEE,* Xu Li, *Member, IEEE,* and Martin Haenggi, *Fellow, IEEE*

***Abstract*—This paper develops an analytical framework for multi-cell uplink NOMA systems based on stochastic geometry. We propose two scenarios for the clustering of NOMA UEs and derive the Laplace transform of the inter-cell interference taking into account uplink power control. We utilize two different ordering techniques, namely mean signal power- (MSP-) and instantaneous signal-to-intercell-interference-and-noise-ratio- (IS$\tilde{\text{I}}$NR-) based, for the successive interference cancellation process at the BSs. For each technique, we present a signal-to-interference-and-noise-ratio (SINR) analysis and derive the transmission success probabilities for the NOMA UEs. We show that uplink power control, which generally reduces the signal power disparity between UEs, does not necessarily degrade the NOMA performance. We discuss how UE clustering and the power control exponent impact this finding. IS$\tilde{\text{I}}$NR-based ordering, which jointly considers path loss, fading, inter-cell interference, and noise, is generally superior to MSP-based ordering. Moreover, we show that the advantage of NOMA vanishes when the target SINR exceeds a certain threshold. A comparison of the two UE clustering scenarios indicates that excluding the UEs which are relatively far from the serving BS may improve the NOMA performance.**

***Index Terms*—Cellular networks, non-orthonogal multiple access, multi-cell, uplink power control, stochastic geometry.**

I. Introduction

In state-of-the-art wireless communication systems like the long-term evolution (LTE), a variety of orthogonal multiple access (OMA) technologies such as orthogonal frequency division multiple access (OFDMA) and single-carrier frequency division multiple access (SC-FDMA) are utilized [1]. While OMA avoids intra-cell interference and retrieves users' signals with a relatively low complexity, the connectivity and data rates are limited by the number of orthogonal resources. To address the requirements of very high data rates and a large number of devices in next-generation (5G) wireless networks [2], non-orthogonal multiple access (NOMA) has received extensive research attention. Contrary to OMA, NOMA serves multiple user equipments (UEs) on the same time-frequency resource block (RB) and thus has the potential to improve the spectral efficiency. The set of UEs served by the same base station (BS) is the NOMA UE cluster. Based on the way messages of the UE cluster are superposed, NOMA is categorized into power-domain NOMA (PD-NOMA) and code-domain NOMA (CD-NOMA). The focus of our work is on PD-NOMA. At the receiver side, successive interference cancellation (SIC) is exploited to separate the messages of the UE cluster [3, 4].

The work was supported in part by the National Key R&D Program of China under Grant 2018YFC0826303 and the Fundamental Research Funds for the Central Universities under Grant 2016JBZ003.

Yanan Liang and Xu Li are with the School of Electronic and Information Engineering, Beijing Jiaotong University, 100044, Beijing, China. (Email:{14111032, xli}@bjtu.edu.cn)

Martin Haenggi is with the Department of Electrical Engineering, University of Notre Dame, Notre Dame, IN 46556 USA. (Email:mhaenggi@nd.edu)

A. Related Work

Extensive studies have been conducted on NOMA-based networks. The performance in terms of outage probability and ergodic sum rate of a downlink NOMA system with randomly deployed UEs is first studied in [5]. [6] investigates the impact of user pairing on the performance of a two-user downlink NOMA system. It is demonstrated that the performance gain of NOMA over OMA can be enlarged by pairing UEs with disparate channel conditions. Furthermore, [7] investigates a dynamic power control scheme to achieve a performance gain over OMA and a good tradeoff betweeen user fairness and system throughput. Closed-form expressions of the outage probability and the achievable sum data rate are derived for a two-user uplink NOMA system in [8], which introduces a power back-off scheme to distinguish multiplexing UEs. The outage probability of uplink NOMA systems serving an arbitrary number of UEs is investigated in [9]. The aforementioned works consider NOMA in single cells and ignore the impact of inter-cell interference, which has a drastic negative impact on the NOMA performance.

Recently, stochastic geometry has been applied as an analytical approach to characterize the performance of multi-cell NOMA systems while accounting for inter-cell interference. The performance of downlink multi-cell NOMA has been well explored [10–14]. In the uplink, however, the analysis is much more complex since the spatial distribution and channel statistics of UEs in interfering cells need to be characterized. Furthermore, the utilization of power control poses significant challenges on the interference analysis. [10, 14, 15] focus on uplink NOMA. Specifically, [10] analyzes the uplink NOMA performance in multi-cell scenarios assuming that the point processes of interfering UEs for each UE in a NOMA cluster are homogeneous Poisson point processes (PPPs) with the same density as the BSs, which is pessimistic since there is no guarantee that one UE is served by each BS under nearest-BS association. [14] extends the model of uplink inter-cell interferers for orthogonal multiple access (OMA) [16], which is approximated as a general PPP with an intensity that depends on the distance from the origin, to the NOMA case and proposes two simplified models for the point process for the spatial locations of inter-cell interferers in uplink NOMA (which we also use in this paper). The moments of the conditional success probability are derived, and an expression for the SIR meta distribution[1] is given. However, [14] does not take into account the SIC chain in the signal-to-interference-ratio analysis and thus overestimates the coverage. In contrast, [15] presents a framework to analyze uplink multi-cell NOMA systems using the Matérn cluster process (MCP), where NOMA UEs are assumed to reside in a disk of fixed radius centered at their serving BS (*i.e.,* the shape and area of the Voronoi cells are ignored for the user placement). The Laplace transform of the intra-cluster and inter-cluster interference are derived, based on which the rate coverage is obtained. However, this model leads to the unrealistic situation where UEs of a NOMA cluster in the typical cell are actually served by other BSs due to the random shape of the Voronoi cells.

In terms of power control, [10] assumes the same average received power for UEs, *i.e.,* full power control, while [14, 15] assume unit transmit power for UEs, *i.e.,* no power control. In uplink NOMA systems, the impact of power control is double-edged. On the one hand, it increases the mean received powers of NOMA UEs (by compensating for the path loss) [18]. On the other hand, it may increase the inter-cell and intra-cell interference (the UEs near the cell edge will use higher power, which increases the intra-cell interference, and some of them may be relatively close to the receiving BSs in adjacent cells, which increases the inter-cell interference) and reduce the difference between NOMA UEs compared to the case of no power control, which degrades the NOMA performance. Therefore, the overall impact of power control in multi-cell uplink NOMA systems needs to be explored in detail.

B. Contributions

In this work we use stochastic geometry to study a large multi-cell uplink NOMA system that takes into account the inter-cell and intra-cell interference, the SIC chain, and power control. We analyze and compare two different UE clustering models, *i.e.,* two location-based schemes to place NOMA UEs in a cluster. With the utilization of a fractional power control scheme, we investigate the performance of mean signal power-(MSP-) based ordering, which is equivalent to distance-based ordering[2], and instantaneous signal-to-intercell-interference-and-noise-ratio- (IS$\tilde{\text{I}}$NR-) based ordering for the SIC process of NOMA UEs. To the best of our knowledge, an analytical work that compares both ordering techniques in uplink NOMA does not exist. Results for an equivalent OMA system are also given to benchmark the gains attained by NOMA. The main contributions of this work are summarized as follows:

- We propose two scenarios for NOMA UE clustering. In the first scenario, the NOMA UEs are distributed uniformly on the in-disk, which is the largest disk centered at the BS that fits inside the Voronoi cell (cf. Fig. 1). Note that the radius of the in-disk is a random variable. This scenario is referred to as the VD (abbreviation of "Voronoi disk") scenario in the following analysis. In the other scenario, the NOMA UEs are distributed uniformly in the Voronoi cell of their serving BS (cf. Fig. 3), which is referred to as the VC (abbreviation of "Voronoi cell") scenario[3].
- We show that, counterintuitively, uplink power control, which generally reduces the signal power disparity between UEs, does not necessarily degrade the NOMA performance. We discuss how UE clustering and the power control exponent impact this finding. Also, we explore what happens if we artificially enhance or over-compensate for the path loss by setting the power control exponent to $\epsilon < 0$ or to $\epsilon > 1$.
- We show that UE ordering based on IS$\tilde{\text{I}}$NR, which takes into account path loss, fading, intercell interference, and noise, is generally superior to MSP-based ordering. However, for a given power control exponent, there may exist a critical level of the target SINR beyond which MSP-based ordering outperforms IS$\tilde{\text{I}}$NR-based ordering.
- We also show that the advantage of NOMA vanishes when the target SINR exceeds a certain threshold. Moreover, a critical minimum level of SIC is required for NOMA to outperform OMA. A comparison of the VD and VC scenarios indicates that excluding the UEs which are relatively far from the serving BS may improve the NOMA performance.

The rest of the work is organized as follows. Section II discusses the VD clustering scenario while Section III discusses the VC scenario. For both scenarios, the Laplace transform of the inter-cell interference and the transmission success probabilities of the NOMA UEs are derived. In Section IV, numerical results of the VD and VC scenarios are given, followed by a comparison of the two scenarios. The concluding remarks are presented in Section V.

II. The VD scenario: UEs reside in the Voronoi disks

A. System Model

We consider an uplink cellular network where BSs are modeled as $\Phi_{\rm b} = \Phi \cup \{o\}$, where $\Phi \subset \mathbb{R}^2$ is a homogeneous PPP with intensity λ. By Slivnyak's theorem [20], the BS at the origin becomes the typical BS serving UEs in the typical cell under expectation over $\Phi_{\rm b}$. In this work we study the performance of the typical cell.

Denote by ρ the distance between the typical BS and its nearest neighbor. Since Φ is a PPP, the distance ρ follows a Rayleigh distribution with probability density function (pdf)

$$f_\rho(x) = 2\pi\lambda x e^{-\pi\lambda x^2}, \quad x \geq 0. \tag{1}$$

Each BS serves N UEs in one time-frequency RB by multiplexing them in the power domain. The UEs, referred to as NOMA UEs, are distributed uniformly on the in-disk, which is the largest disk centered at the BS that fits inside the

[1] See [17] for the definition.

[2] See [19] for a detailed explanation.

[3] The VC scenario can be viewed as a benchmark scenario for multi-cell uplink NOMA systems.

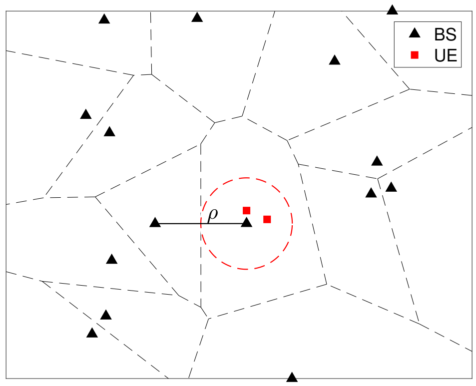

Fig. 1. A realization of the network with $N = 2$ for the VD scenario. The in-disk for the typical cell is marked by the dashed circle.

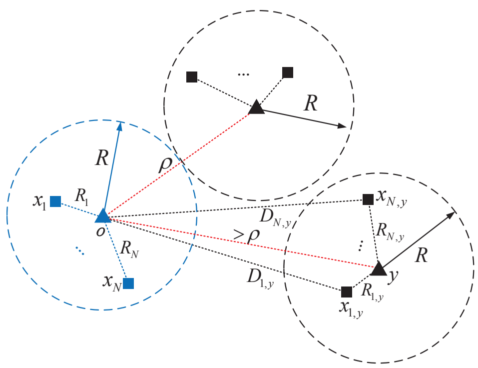

Fig. 2. Uplink network model for the VD scenario. N UEs are uniformly distributed on a disk of radius $R = \rho/2$ centered at each BS. The typical BS is at the origin, and the typical UEs served by it are at $x_i\,(1 \le i \le N)$. ρ denotes the distance between the typical BS and its nearest neighbor.

Voronoi cell. The UEs outside the disk are relatively far from their serving BS and thus are better served on their own RB or using coordinated multi-point (CoMP) transmission [21]. The radius of the in-disk is denoted as $R = \rho/2$.

Approximation 1. We assume that in each cell, there are N UEs distributed uniformly in the disk centered at the BS with the same radius $R = \rho/2$. Hence we ignore that the radii of the in-disks in interfering cells are different from that of the typical cell. Using the actual radii would render the analysis prohibitively complex. Then, given ρ, the user point process is a Poisson cluster process (PCP) with N points distributed uniformly and independently in each cluster.

The interfering UEs seen from the typical BS are modeled as $\Phi_{\rm I} = \bigcup_{y\in\Phi}\mathcal{N}^y$, where $\mathcal{N}^y$ denotes the set of UEs whose serving BS is at location y. A realization of the cell at o, its in-disk, and the surrounding cells are shown in Fig. 1. In the typical cell, the locations of UEs are denoted as $x_i\,(1 \le i \le N)$, as shown in Fig. 2. The link distances from the typical UE x_i to the typical BS at o are denoted as R_i. In the interfering cell whose serving BS is at y, the locations of UEs are denoted as $x_{i,y}$, and the link distances are denoted as $R_{i,y}$.

Given ρ, the link distances $R_i\,(1 \le i \le N)$ in the typical cell are identically and independently distributed (i.i.d.) with pdf[4]

$$f_{R_i|\rho}(r|\rho) = \frac{8r}{\rho^2}, \quad 0 \le r \le \frac{\rho}{2}. \tag{2}$$

The link distances $R_{i,y}\,(1 \le i \le N)$ follow the same distribution as R_i.

The standard power-law path loss model with exponent $\alpha > 2$ for signal propagation and the standard Rayleigh fading are used. The power fading coefficients h_{x_i} associated with the user at x_i and the typical BS are exponentially distributed variables with unit mean, *i.e.*, $h_{x_i} \sim \exp(1)$. The same follows for $h_{x_{i,y}}$. We assume h_{x_i} and $h_{x_{i,y}}$ are independent for all $x_i \in \mathcal{N}^o$ and $x_{i,y} \in \Phi_{\rm I}$.

We use fractional power control in the form $P_i = P_0 R_i^{\alpha\epsilon}$ for the typical UEs and $P_{i,y} = P_0 R_{i,y}^{\alpha\epsilon}$ for the interfering UEs, which is one of the most widely used schemes for uplink cellular networks to partially compensate for the path loss. ϵ denotes the power control exponent. In addition to the usual range $\epsilon \in [0,1]$, we also consider the cases of $\epsilon < 0$ and $\epsilon > 1$ to explore what happens if we artificially enhance or overcompensate for the path loss. P_0 denotes the baseline transmit power when there is no power control. Without loss of generality, we assume $P_0 = 1$. The noise power is denoted as σ^2.

B. LT of the Inter-Cell Interference

Approximation 2. In the analysis of the inter-cell interference in the uplink case, we need to consider the distances from the interfering UEs to the typical BS. Since both the distances from the interfering UEs to their serving BS (*i.e.*, $R_{i,y}$) and the distances from other BSs to the typical BS (*i.e.*, $\|y\|$) are random variables, the analysis of the distances from interfering UEs to the typical BS (*i.e.*, $D_{i,y}$) is rather difficult. To make the analysis tractable, we use an approximation that the interfering UEs are all located at their serving BS's location in the analysis of the inter-cell interference[5]. Note that the interfering UEs are still using the transmit power determined by their actual location.

Lemma 1. *In the VD scenario under Approximations 1 and 2, the Laplace transform (LT) of the inter-cell interference conditioned on ρ is given as*

$$\mathcal{L}_{I^\star|\rho}(s) \approx \exp\left(-2\pi\lambda\int_\rho^\infty \left(1-\left(V_\epsilon(y)\right)^N\right)y\mathrm{d}y\right)\cdot\left(V_\epsilon(\rho)\right)^N, \tag{3}$$

where $V_\epsilon(y) \triangleq {}_2F_1(1, \frac{\delta}{\epsilon}; 1+\frac{\delta}{\epsilon}; -s\left(\frac{\rho}{2}\right)^{\alpha\epsilon}y^{-\alpha})$, $\delta \triangleq \frac{2}{\alpha}$, *and* $\epsilon > 0$. *For the case of* $\epsilon = 0$, *the LT of* $I^\star$ *is simplified as*

$$\mathcal{L}_{I^\star|\rho}(s) \approx \exp\left(-2\pi\lambda\int_\rho^\infty\left(1-\frac{1}{(1+sy^{-\alpha})^N}\right)y\mathrm{d}y\right)\cdot\frac{1}{(1+s\rho^{-\alpha})^N}. \tag{4}$$

Proof. See Appendix A. □

[4]Note that our model is different from the MCP model in that ρ is a random variable affected by the shape and area of the Voronoi cells. Our model ensures that the typical NOMA UEs are exclusively served by the typical BS.

[5][11] uses a similar approximation in downlink NOMA that assumes the UEs are at their serving BS's location. It is their average location since the UEs are uniformly distributed on the in-disk.

Approximation 3. To simplify (3), we use the average power $\bar{P}$ to replace $P_{i,y}$ for all $1 \leq i \leq N$ and $y \in \Phi$ as an approximation, which is given as

$$\bar{P} = \int_0^{\frac{\rho}{2}} x^{\alpha\epsilon} \frac{8x}{\rho^2} \mathrm{d}x = \frac{2}{\alpha\epsilon + 2} \Big(\frac{\rho}{2}\Big)^{\alpha\epsilon} = \frac{\delta}{\epsilon + \delta} \Big(\frac{\rho}{2}\Big)^{\alpha\epsilon}, \quad (5)$$

valid for $\epsilon > -\delta$.

Corollary 1. *Assuming average transmit power for the interfering UEs, the LT of the inter-cell interference is approximated as*

$$\begin{aligned} &\mathcal{L}_{I^\star|\rho}(s) \\ &\approx \exp\Big(-\sum_{k=1}^{N} \tbinom{N}{k} W_k(\rho) s^k {}_2F_1\Big(k, k-\delta; k+1-\delta; -\frac{s\bar{P}}{\rho^\alpha}\Big)\Big) \\ &\quad \cdot \frac{1}{(1 + s\bar{P}\rho^{-\alpha})^N}, \end{aligned} \quad (6)$$

where $W_k(\rho) = \frac{\pi\lambda\delta(-1)^{k+1}\bar{P}^k}{(k-\delta)\rho^{\alpha(k-\delta)}}$ *and* $\epsilon > -\delta$.

Proof. See Appendix B. □

C. Transmission Success Probabilities

Next we analyze the transmission success probabilities of the N NOMA UEs in the typical cell. SIC is employed for decoding NOMA UEs, which requires the ordering of UEs based on the link quality. We order UEs in such a way that the i^{th} UE, which is denoted as U_i, has the i^{th} strongest link. Here, we consider two link quality metrics, namely:

- Mean signal power (MSP): the MSP of the typical UEs are $P_i' = h_i R_i^{-(1-\epsilon)\alpha}$ given the fractional power control scheme $P_i = R_i^{\alpha\epsilon}$. Therefore, in MSP-based ordering, the typical UEs are indexed according to their ascending ordered link distance $\hat{R}_i$ with $\hat{R}_1 < ... < \hat{R}_N$ under the condition $\epsilon < 1$,[6] *i.e.,* the i^{th} closest UE from the origin is referred to as U_i.
- Instantaneous signal-to-intercell-interference-and-noise-ratio (IS$\tilde{\text{I}}$NR): the IS$\tilde{\text{I}}$NR of the typical UEs are $Z_i = \frac{h_i R_i^{-(1-\epsilon)\alpha}}{I^\star + \sigma^2}$. In IS$\tilde{\text{I}}$NR-based ordering, the typical UEs are indexed with respect to their descending ordered IS$\tilde{\text{I}}$NR $\hat{Z}_i$, *i.e.,* U_i has the i^{th} largest IS$\tilde{\text{I}}$NR.

If SIC is ideal[7], *i.e.,* there is no residual interference, the SINR of U_i for $1 \leq i \leq N$ is

$$\mathrm{SINR}_i = \frac{h_i R_i^{-(1-\epsilon)\alpha}}{\sum\limits_{j=i+1}^{N} h_j R_j^{-(1-\epsilon)\alpha} + I^\star + \sigma^2}. \quad (7)$$

To decode U_i's message, the BS needs to successfully decode the messages of UEs whose order indexes are smaller than i. We use θ_i to denote the target SINR (*i.e.,* the SINR threshold corresponding to the target rate) of U_i. Then the transmission success (sometimes also called coverage) of U_i is defined as the joint event

$$C_i = \bigcap_{k=1}^{i} \{\mathrm{SINR}_k > \theta_k\}. \quad (8)$$

Theorem 1. *In the VD scenario, the transmission success probability of* $\mathrm{U}_i, 1 \leq i \leq N$ *using MSP-based ordering is given as*

$$\mathbb{P}(C_i) = \mathbb{E}_\rho \Big[\mathbb{E}_{\hat{R}_1,\ldots,\hat{R}_N} \Big[\prod_{k=1}^{i} a_k \prod_{j=i+1}^{N} b_{i,j} e^{-\sigma^2 d_i} \mathcal{L}_{I^\star|\rho}(d_i) \Big] \Big], \quad (9)$$

where

$$a_k = \begin{cases} \dfrac{1}{1 + \sum_{t=1}^{k-1} \theta_t \prod_{q=t+1}^{k-1} (1+\theta_q) \hat{R}_t^{(1-\epsilon)\alpha} \hat{R}_k^{-(1-\epsilon)\alpha}}, & \epsilon \leq 1, \\ \dfrac{1}{1 + \sum_{t=1}^{k-1} \theta_t \prod_{q=t+1}^{k-1} (1+\theta_q) \hat{R}_{N+1-t}^{(1-\epsilon)\alpha} \hat{R}_{N+1-k}^{-(1-\epsilon)\alpha}}, & \epsilon > 1, \end{cases} \quad (10)$$

$$b_{i,j} = \begin{cases} \dfrac{1}{1 + \sum_{t=1}^{i} \theta_t \prod_{q=t+1}^{i} (1+\theta_q) \hat{R}_t^{(1-\epsilon)\alpha} \hat{R}_j^{-(1-\epsilon)\alpha}}, & \epsilon \leq 1, \\ \dfrac{1}{1 + \sum_{t=1}^{i} \theta_t \prod_{q=t+1}^{i} (1+\theta_q) \hat{R}_{N+1-t}^{(1-\epsilon)\alpha} \hat{R}_{N+1-j}^{-(1-\epsilon)\alpha}}, & \epsilon > 1, \end{cases} \quad (11)$$

$$d_i = \begin{cases} \sum\limits_{t=1}^{i} \theta_t \prod\limits_{q=t+1}^{i} (1+\theta_q) \hat{R}_t^{(1-\epsilon)\alpha}, & \epsilon \leq 1, \\ \sum\limits_{t=1}^{i} \theta_t \prod\limits_{q=t+1}^{i} (1+\theta_q) \hat{R}_{N+1-t}^{(1-\epsilon)\alpha}, & \epsilon > 1, \end{cases} \quad (12)$$

for $1 \leq k \leq i$, $i+1 \leq j \leq N$ *and* $1 \leq i \leq N$.

Proof. See Appendix C. □

Corollary 2. *For* $N = 2$ *in the VD scenario, the transmission success probability of* U_1 *using MSP-based ordering is given as*

$$\mathbb{P}(C_1) = \begin{cases} \displaystyle\int_0^\infty \int_0^{\frac{x}{2}} F_\epsilon(x,r) \mathcal{L}_{I^\star|x}(\theta_1 r^{\frac{2}{\delta_\epsilon}}) T_\epsilon(x,r) \mathrm{d}r f_\rho(x) \mathrm{d}x, & \epsilon < 1, \\ \displaystyle\int_0^\infty \int_0^{\frac{x}{2}} (-\tau_\epsilon) r^2 F_\epsilon(x,r) \mathcal{L}_{I^\star|x}(\theta_1 r^{\frac{2}{\delta_\epsilon}}) \mathrm{d}r f_\rho(x) \mathrm{d}x, & \epsilon > 1, \\ \displaystyle\int_0^\infty \frac{e^{-\theta_1\sigma^2} \mathcal{L}_{I^\star|x}(\theta_1)}{1+\theta_1} f_\rho(x) \mathrm{d}x, & \epsilon = 1, \end{cases} \quad (13)$$

where $F_\epsilon(x,r) \triangleq 64\delta_\epsilon r x^{-4} e^{-\theta_1\sigma^2 r^{\frac{2}{\delta_\epsilon}}}$, $\delta_\epsilon \triangleq \frac{2}{(1-\epsilon)\alpha}$, $\tau_\epsilon \triangleq \int_0^1 \frac{v^{-\delta_\epsilon - 1}}{1+\theta_1 v} \mathrm{d}v$, *and*

$$T_\epsilon(x,r) \triangleq \int_{(\frac{x}{2})^{-\frac{2}{\delta_\epsilon}}}^{r^{-\frac{2}{\delta_\epsilon}}} \frac{v^{-\delta_\epsilon-1}}{1+\theta_1 r^{\frac{2}{\delta_\epsilon}} v} \mathrm{d}v. \quad (14)$$

[6] In the case of $\epsilon > 1$, the typical UEs are indexed according to their descending ordered link distance $\hat{R}_i$. In the case of $\epsilon = 1$, *i.e.,* full power control, the MSPs of the NOMA UEs are the same, therefore the decoding order does not matter. Without loss of generality, we take into account the distances from the NOMA UEs to the BS and decode the UE nearer to the BS first.

[7] Here we assume ideal SIC under the assumption of perfect channel estimation to illustrate the analytical model more coherently. We analyze the impact of imperfect SIC on NOMA systems in Appendix E.

For U_2*, it is given as*

$$\mathbb{P}(C_2)=\begin{cases}\int\limits_0^{\infty}\int\limits_0^{\frac{x}{2}}\int\limits_{r_1}^{\frac{x}{2}}\frac{G_\epsilon(x,r_1,r_2)\mathcal{L}_{I^\star|x}(v_\epsilon(r_1,r_2))}{1+\theta_1 r_1^{\frac{2}{\delta_\epsilon}}r_2^{-\frac{2}{\delta_\epsilon}}}\mathrm{d}r_2\mathrm{d}r_1 f_\rho(x)\mathrm{d}x, & \\ \hfill \epsilon<1, & \\ \int\limits_0^{\infty}\int\limits_0^{\frac{x}{2}}\int\limits_0^{r_2}\frac{G_\epsilon(x,r_2,r_1)\mathcal{L}_{I^\star|x}(v_\epsilon(r_2,r_1))}{1+\theta_1 r_2^{\frac{2}{\delta_\epsilon}}r_1^{-\frac{2}{\delta_\epsilon}}}\mathrm{d}r_1\mathrm{d}r_2 f_\rho(x)\mathrm{d}x, & \\ \hfill \epsilon>1, & \\ \int\limits_0^{\infty}\frac{e^{-(\theta_2+\theta_1(1+\theta_2))\sigma^2}\mathcal{L}_{I^\star|x}((\theta_2+\theta_1(1+\theta_2)))}{1+\theta_1}f_\rho(x)\mathrm{d}x, & \\ \hfill \epsilon=1, & \end{cases} \tag{15}$$

where $G_\epsilon(x,r_1,r_2) \triangleq 128 r_1 r_2 x^{-4} e^{-\sigma^2 v_\epsilon(r_1,r_2)}$ *and* $v_\epsilon(r_1,r_2)\triangleq\theta_2 r_2^{\frac{2}{\delta_\epsilon}}+\theta_1(1+\theta_2)r_1^{\frac{2}{\delta_\epsilon}}$.

Proof. See Appendix D. □

For IS$\tilde{\text{I}}$NR-based ordering, the transmission success probability of $\mathrm{U}_i, 1\le i\le N$ is

$$\begin{aligned}&\mathbb{P}(C_i)\\&=\mathbb{P}\left[\frac{\hat{Z}_1}{\sum\limits_{j=2}^{N}\hat{Z}_j+1}>\theta_1,...,\frac{\hat{Z}_i}{\sum\limits_{j=i+1}^{N}\hat{Z}_j+1}>\theta_i \mid \hat{Z}_1>\cdots>\hat{Z}_N\right]\\&\overset{(a)}{=}\mathbb{E}\Big[\int_0^\infty \mathrm{d}z_N\cdots\int_0^\infty \mathrm{d}z_{i+1}\int_{\min(z_{i+1},\theta_i(\sum\limits_{j=i+1}^{N}z_j+1))}^{\infty}\mathrm{d}z_i\cdots\\&\qquad\times\int_{\min(z_2,\theta_1(\sum\limits_{j=2}^{N}z_j+1))}^{\infty}\mathrm{d}z_1 n! f_{\hat{Z}_1}(z_1)\cdots f_{\hat{Z}_N}(z_N)\Big],\end{aligned} \tag{16}$$

where (a) follows from the independence of $\hat{Z}_i$ for $1\le i\le N$ and $f_{\hat{Z}_1,...,\hat{Z}_N}(z_1,...,z_N)=n!f_{\hat{Z}_1}(z_1)\cdots f_{\hat{Z}_N}(z_N)$ based on order statistics [22].

For $N\ge 3$, the expressions of $\mathbb{P}(C_i)$ are too complex. To illustrate the analytical model more briefly and coherently, we focus on $N=2$ for IS$\tilde{\text{I}}$NR-based ordering.

Theorem 2. *For* $N=2$ *in the VD scenario, the transmission success probabilities of* U_1 *and* U_2 *using IS$\tilde{\text{I}}$NR-based ordering for* $\theta_1\ge 1$ *are given as*

$$\mathbb{P}(C_1)=\int_0^\infty\int_0^\infty 2J(\theta_1 z+\theta_1,x)K(z,x)\mathrm{d}z f_\rho(x)\mathrm{d}x, \tag{17}$$

$$\mathbb{P}(C_2)=\int_0^\infty\int_{\theta_2}^\infty 2J(\theta_1 z+\theta_1,x)K(z,x)\mathrm{d}z f_\rho(x)\mathrm{d}x, \tag{18}$$

while for $\theta_1<1$ *they are given as*

$$\begin{aligned}\mathbb{P}(C_1)=\int_0^\infty\Big(&\int_0^{\frac{\theta_1}{1-\theta_1}}2J(\theta_1 z+\theta_1,x)K(z,x)\mathrm{d}z\\&+\int_{\frac{\theta_1}{1-\theta_1}}^\infty 2J(z,x)K(z,x)\mathrm{d}z\Big)f_\rho(x)\mathrm{d}x,\end{aligned} \tag{19}$$

$$\begin{aligned}\mathbb{P}(C_2)=\int_0^\infty\Big(&\int_{\min(\theta_2,\frac{\theta_1}{1-\theta_1})}^{\frac{\theta_1}{1-\theta_1}}2J(\theta_1 z+\theta_1,x)K(z,x)\mathrm{d}z\\&+\int_{\frac{\theta_1}{1-\theta_1}}^\infty 2J(z,x)K(z,x)\mathrm{d}z\Big)f_\rho(x)\mathrm{d}x,\end{aligned} \tag{20}$$

where

$$J(z,x)=\int_0^{\frac{x}{2}}8rx^{-2}\exp(-z\sigma^2 r^{(1-\epsilon)\alpha})\mathcal{L}_{I^\star|x}(zr^{(1-\epsilon)\alpha})\mathrm{d}r, \tag{21}$$

$$\begin{aligned}K(z,x)=\int_0^{\frac{x}{2}}&8r^{1+(1-\epsilon)\alpha}x^{-2}\exp(-z\sigma^2 r^{(1-\epsilon)\alpha})\\&\cdot\Big(\sigma^2\mathcal{L}_{I^\star|x}(zr^{(1-\epsilon)\alpha})-\mathcal{L}'_{I^\star|x}(zr^{(1-\epsilon)\alpha})\Big)\mathrm{d}r,\end{aligned} \tag{22}$$

in which $\mathcal{L}'_{I^\star|x}(s)=\mathrm{d}\mathcal{L}_{I^\star|x}(s)/\mathrm{d}s$.

Proof. See Appendix F. □

D. NOMA Gain

In the OMA case, the LT of the inter-cell interference I° is obtained by assuming $N=1$, *i.e.,* $\mathcal{L}_{I^\circ|x}(s)=\mathcal{L}_{I^\star|x}(s)|_{N=1}$.

Let θ denote the target SINR of the OMA UE. The transmission success probability of the typical OMA UE is

$$\begin{aligned}\mathbb{P}(C)&=\mathbb{P}\Big[\frac{h_1 R_1^{-(1-\epsilon)\alpha}}{I^\circ+\sigma^2}>\theta\Big]\\&=\mathbb{E}_\rho\Big[\mathbb{E}_{R_1}\Big[e^{-\theta\sigma^2 R_1^{(1-\epsilon)\alpha}}\mathcal{L}_{I^\circ|\rho}(\theta R_1^{(1-\epsilon)\alpha})\Big]\Big]\\&=\int_0^\infty\int_0^{\frac{x}{2}}8rx^{-2}e^{-\theta\sigma^2 r^{(1-\epsilon)\alpha}}\mathcal{L}_{I^\circ|x}(\theta r^{(1-\epsilon)\alpha})\mathrm{d}r f_\rho(x)\mathrm{d}x.\end{aligned} \tag{23}$$

We use $\mathcal{R}_{\mathrm{NOMA}}$ and $\mathcal{R}_{\mathrm{OMA}}$ to denote the achievable transmission sum rate of NOMA and OMA, respectively, and define the uplink NOMA gain G as

$$\begin{aligned}G&\triangleq\mathcal{R}_{\mathrm{NOMA}}-\mathcal{R}_{\mathrm{OMA}}\\&=\sum_{i=1}^{N}\mathbb{P}(C_i)\log(1+\theta_i)-\mathbb{P}(C)\log(1+\theta).\end{aligned} \tag{24}$$

For $N=2$, $\mathbb{P}(C_1)$ and $\mathbb{P}(C_2)$ are given in (13) and (15) for MSP-based ordering and in (17)-(20) for IS$\tilde{\text{I}}$NR-based ordering.

III. The VC scenario: UEs reside in the Voronoi cells

A. System Model

In the VC scenario, we also model the BSs as $\Phi_{\mathrm{b}}=\Phi\cup\{o\}$, in which $\Phi\subset\mathbb{R}^2$ is a homogeneous PPP with intensity λ. By Slivnyak's theorem, the BS at the origin becomes the typical BS under expectation over Φ_{b}. Assume that N NOMA UEs are served on one RB by each BS. A realization of the cell at o, the UEs in it, and the surrounding cells are shown in Fig. 3. The UEs in the typical cell are denoted as x_i, $1\le i\le N$, as depicted in Fig. 4. The link distances from UE x_i to the typical BS are denoted as R_i. From the results in [16], the R_i are distributed as

$$f_{R_i}(r)=2a\pi\lambda r\exp\left(-a\pi\lambda r^2\right), \quad r>0, \tag{25}$$

where a is the correction factor relative to the distribution in the Crofton cell. The value $a=9/7$ is used in the following analysis.

To characterize the inter-cell interference, we consider two approximative models based on the pair correlation function between the interfering UEs and the typical BS [14].

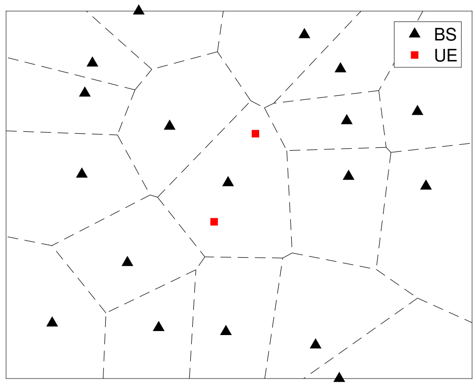

Fig. 3. A realization of the network with $N = 2$ for the VC scenario.

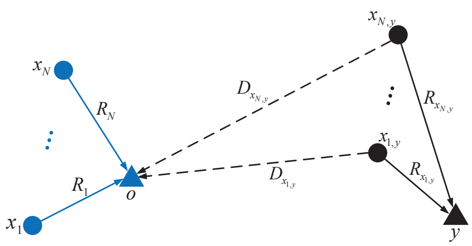

Fig. 4. Uplink network model for the VC scenario. N NOMA UEs are served on a given RB in each cell.

1) Model 1: The interfering UE process for the typical NOMA UEs is denoted as $\Psi_{\rm I}$, which is formally defined as $\Psi_{\rm I} = \{y \in \Phi : U_N(V(y))\}$, where $V(y)$ denotes the Voronoi cell of BS y. $U_N(B), B \subset \mathbb{R}^2$, denotes a set of N points chosen uniformly and randomly from B, and independently across different B. In the interfering cell whose serving BS is located at y, the locations of UEs are denoted as $x_{i,y}$ for $1 \leq i \leq N$, and their link distances are denoted as $R_{x_{i,y}}$. The distances from the interfering UEs to the typical BS are denoted as $D_{x_{i,y}} = \|x_{i,y}\|$. Since $R_{x_{i,y}}$ cannot be larger than $D_{x_{i,y}}$ (due to nearest-BS association), the distribution of $R_{x_{i,y}}$ conditioned on $D_{x_{i,y}}$ is given as

$$f_{R_{x_{i,y}}}(r|D_{x_{i,y}}) = \frac{2a\pi\lambda r\exp\left(-a\pi\lambda r^2\right)}{1-\exp\left(-a\pi\lambda D_{x_{i,y}}^2\right)}, \quad 0 < r < D_{x_{i,y}}. \tag{26}$$

Based on the results in [16], $\Psi_{\rm I}$ is approximated as a PPP with intensity function

$$\lambda(x) = N\lambda(1-\exp(-b\pi\lambda\|x\|^2)), \tag{27}$$

where $b = 12/5$.

2) Model 2: The inter-cell interfering UEs are modeled as a PCP, where the parents form an inhomogeneous PPP $\Psi_{\rm p}$ with intensity function $\lambda_{\rm p}(x) = \lambda(1-\exp(-b\pi\lambda\|x\|^2))$ while the N offspring points in each cluster are located at the same location as the parent[8].

[8]Note that the purpose of Model 2 is to approximate the interferers' point process by a tractable simplified model. The locations of the NOMA UEs under consideration (those in the typical cell that are to be decoded at their base station) are placed according to the PCP model, *i.e.,* they are not assumed co-located.

As in Section II-A, we assume the standard power-law path loss model with exponent $\alpha > 2$ for signal propagation and the standard Rayleigh fading. Fractional power control in the form $P = R^{\alpha\epsilon}$ is used for all UEs. In addition to the usual interval $\epsilon \in [0,1]$, we also consider the cases of $\epsilon < 0$ and $\epsilon > 1$ to explore what happens if we artificially enhance or overcompensate for the path loss.

B. LT of the Inter-Cell Interference

Lemma 2. *In the VC scenario, the LT of the inter-cell interference is approximated as*

$$\mathcal{L}_{I^*}(s) \approx \exp\left(-2\pi N\lambda\int_0^\infty\left(1-e^{-b\pi\lambda z^2}\right)(1-\mu_1(z,s))z{\rm d}z\right), \tag{28}$$

for Model 1 and

$$\mathcal{L}_{I^*}(s) \approx \exp\left(-2\pi\lambda\int_0^\infty\left(1-e^{-b\pi\lambda z^2}\right)(1-\mu_N(z,s))z{\rm d}z\right), \tag{29}$$

for Model 2, where

$$\mu_n(z,s) \triangleq \int_0^z \frac{2a\pi\lambda y e^{-a\pi\lambda y^2}}{(1-e^{-a\pi\lambda z^2})(1+sy^{\epsilon\alpha}z^{-\alpha})^n}{\rm d}y. \tag{30}$$

Proof. See Appendix G. □

C. Transmission Success Probabilities

Theorem 3. *In the VC scenario, the transmission success probability of* $\mathrm{U}_i, 1 \leq i \leq N$ *using MSP-based ordering is given as*

$$\mathbb{P}(C_i) = \mathbb{E}_{\hat{R}_1,\ldots,\hat{R}_N}\left[\prod_{k=1}^{i} a_k \prod_{j=i+1}^{N} b_{i,j} e^{-\sigma^2 d_i}\mathcal{L}_{I^*}(d_i)\right], \tag{31}$$

where a_k*,* b_k*, and* d_k *are given in* (10)*,* (11)*, and* (12)*, respectively.*

Proof. The proof is similar to that of Theorem 1 (see Appendix C). □

Corollary 3. *For* $N = 2$ *in the VC scenario, the transmission success probability of* U_1 *using MSP-based ordering for* $\epsilon < 1$ *is given as*

$$\mathbb{P}(C_1) = \begin{cases} \displaystyle\int_0^\infty 2e^{-\theta_1\sigma^2 r^{\frac{2}{\delta_\epsilon}}}\mathcal{L}_{I^*}(\theta_1 r^{\frac{2}{\delta_\epsilon}})\xi_{\delta_\epsilon}(a\pi\lambda r^2,\theta_1)2a\pi\lambda r e^{-a\pi\lambda r^2}{\rm d}r, & \epsilon < 1, \\ \displaystyle\int_0^\infty 2e^{-\theta_1\sigma^2 r^{\frac{2}{\delta_\epsilon}}}\mathcal{L}_{I^*}(\theta_1 r^{\frac{2}{\delta_\epsilon}})(-\xi_{\delta_\epsilon}(a\pi\lambda r^2,\theta_1))2a\pi\lambda r e^{-a\pi\lambda r^2}{\rm d}r, & \epsilon > 1, \\ \dfrac{e^{-\theta_1\sigma^2}\mathcal{L}_{I^*}(\theta_1)}{1+\theta_1}, & \epsilon = 1, \end{cases} \tag{32}$$

where

$$\xi_{\delta_\epsilon}(y,z) \triangleq \delta_\epsilon y\int_0^1 \frac{v^{-\delta_\epsilon-1}e^{-yv^{-\delta_\epsilon}}}{1+zv}{\rm d}v. \tag{33}$$

For U_2*, it is given as*

$$\mathbb{P}(C_2) = \begin{cases} \displaystyle\int_0^{\infty}\int_{r_1}^{\infty} \frac{M(r_1,r_2)e^{-\sigma^2 v_\epsilon(r_1,r_2)}\mathcal{L}_{I^*}(v_\epsilon(r_1,r_2))}{1+\theta_1 r_1^{\frac{2}{\delta_\epsilon}} r_2^{-\frac{2}{\delta_\epsilon}}}\mathrm{d}r_2\mathrm{d}r_1, & \epsilon<1, \\ \displaystyle\int_0^{\infty}\int_{0}^{r_2} \frac{M(r_2,r_1)e^{-\sigma^2 v_\epsilon(r_2,r_1)}\mathcal{L}_{I^*}(v_\epsilon(r_2,r_1))}{1+\theta_1 r_2^{\frac{2}{\delta_\epsilon}} r_1^{-\frac{2}{\delta_\epsilon}}}\mathrm{d}r_1\mathrm{d}r_2, & \epsilon>1, \\ \displaystyle\frac{e^{-(\theta_2+\theta_1(1+\theta_2))\sigma^2}\mathcal{L}_{I^*}(\theta_2+\theta_1(1+\theta_2))}{1+\theta_1}, \quad \epsilon=1, & \end{cases} \tag{34}$$

where $M(r_1,r_2) \triangleq 8(a\pi\lambda)^2 r_1 r_2 e^{-a\pi\lambda(r_1^2+r_2^2)}$ *and* $v_\epsilon(r_1,r_2)$ *is defined in Corollary 2.*

Proof. See Appendix H. □

Theorem 4. *For* $N=2$ *in the VC scenario, the transmission success probabilities of* U_1 *and* U_2 *using IS$\tilde{\text{I}}$NR-based ordering for* $\theta_1 \geq 1$ *are given as*

$$\mathbb{P}(C_1) = \int_0^{\infty} 2J'(\theta_1 z+\theta_1)K'(z)\mathrm{d}z, \tag{35}$$

$$\mathbb{P}(C_2) = \int_{\theta_2}^{\infty} 2J'(\theta_1 z+\theta_1)K'(z)\mathrm{d}z, \tag{36}$$

while for $\theta_1<1$ *they are given as*

$$\mathbb{P}(C_1) = \int_0^{\frac{\theta_1}{1-\theta_1}} 2J'(\theta_1 z+\theta_1)K'(z)\mathrm{d}z + \int_{\frac{\theta_1}{1-\theta_1}}^{\infty} 2J'(z)K'(z)\mathrm{d}z, \tag{37}$$

$$\mathbb{P}(C_2) = \int_{\min(\theta_2,\frac{\theta_1}{1-\theta_1})}^{\frac{\theta_1}{1-\theta_1}} 2J'(\theta_1 z+\theta_1)K'(z)\mathrm{d}z + \int_{\frac{\theta_1}{1-\theta_1}}^{\infty} 2J'(z)K'(z)\mathrm{d}z, \tag{38}$$

where

$$J'(z) = \int_0^{\infty} \exp(-z\sigma^2 r^{\frac{2}{\delta_\epsilon}})\mathcal{L}_{I^*}(zr^{\frac{2}{\delta_\epsilon}})2a\pi\lambda r e^{-a\pi\lambda r^2}\mathrm{d}r, \tag{39}$$

$$K'(z) = \int_0^{\infty} \exp(-z\sigma^2 r^{\frac{2}{\delta_\epsilon}})\left(\sigma^2\mathcal{L}_{I^*}(zr^{\frac{2}{\delta_\epsilon}}) - \mathcal{L}'_{I^*}(zr^{\frac{2}{\delta_\epsilon}})\right) \cdot 2a\pi\lambda r^{1+\frac{2}{\delta_\epsilon}}e^{-a\pi\lambda r^2}\mathrm{d}r, \tag{40}$$

in which $\mathcal{L}'_{I^*}(s) = \mathrm{d}\mathcal{L}_{I^*}(s)/\mathrm{d}s$*.*

Proof. See Appendix I. □

D. NOMA Gain

In the OMA case, the LT of the inter-cell interference $I^\diamond$ is obtained by assuming $N=1$, *i.e.*, $\mathcal{L}_{I^\diamond|x}(s) = \mathcal{L}_{I^*|x}(s)|_{N=1}$.

Thus the transmission success probability of the typical OMA UE is given as

$$\mathbb{P}(C) = \mathbb{P}\left[\frac{h_1 R_1^{-(1-\epsilon)\alpha}}{I^\diamond+\sigma^2} > \theta\right] = \int_0^{\infty} e^{-\theta\sigma^2 r^{(1-\epsilon)\alpha}}\mathcal{L}_{I^\diamond}(\theta r^{(1-\epsilon)\alpha})2a\pi\lambda r e^{-a\pi\lambda r^2}\mathrm{d}r. \tag{41}$$

Similar as in the VD scenario, the NOMA gain given in (24) is considered. For $N=2$, $\mathbb{P}(C_1)$ and $\mathbb{P}(C_2)$ for the VC scenario are given in (32) and (34) assuming MSP-based ordering and in (35)-(38) assuming IS$\tilde{\text{I}}$NR-based ordering.

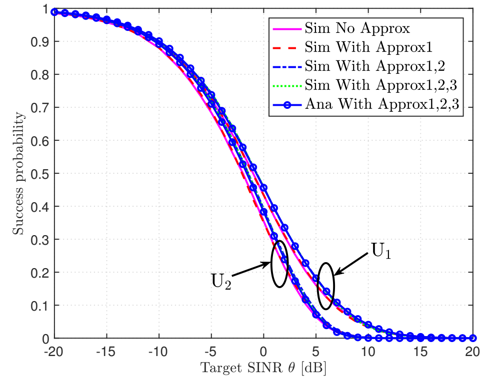

(a) MSP-based ordering

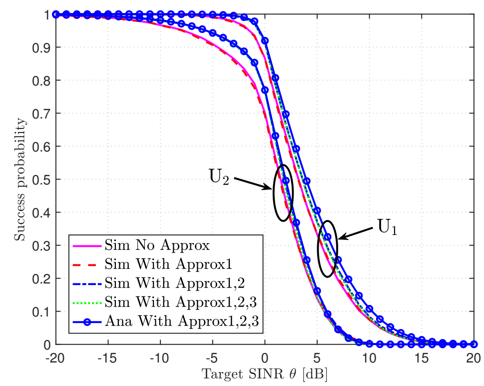

(b) IS$\tilde{\text{I}}$NR-based ordering

Fig. 5. Comparison of the analytical and simulation results for the transmission success probabilities of the NOMA UEs for $N=2$ under different simplifying assumptions in the VD scenario. $\lambda=1$, $\epsilon=1$, $\alpha=4$, $\sigma^2=0.01, \theta_1=\theta_2=\theta$ are assumed.

IV. Numerical Results

A. The VD Scenario

First, we show that the simplifying assumptions (Approximations 1-3) we make in the analysis of the VD scenario are sensible and result in tight approximative results. Fig. 5 denotes the transmission success probabilities of the NOMA UEs in the typical cell for both ordering techniques, which are obtained based on the analytical results under Approximations 1-3 and the simulation results under different approximations. It is indicated that Approximation 2 (assuming the interfering UEs are at their serving BSs' locations), leads to a slightly larger deviation than the other approximations. Overall, the assumptions are mild and sensible.

Assuming perfect SIC and the same target SINR for the NOMA UEs, we explore the impact of ϵ on NOMA systems. Fig. 6 depicts the transmission success probabilities of the NOMA UEs using MSP- and IS$\tilde{\text{I}}$NR-based ordering for different values of $\epsilon \in [0,1]$ assuming $N=2$. The curves correspond to the analytical results given in Corollary 2 and Theorem 2 while the markers correspond to the simulation results. It is shown that the transmission success probabilities of U_1 and U_2 deteriorate with the increase of ϵ for all values

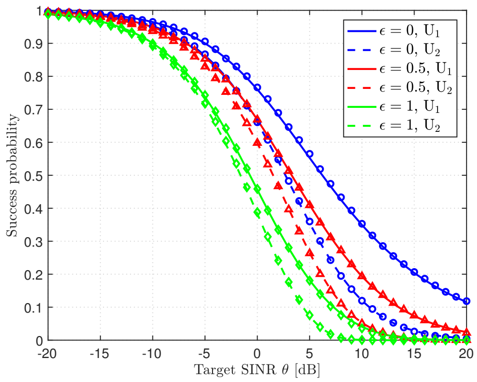

(a) MSP-based ordering

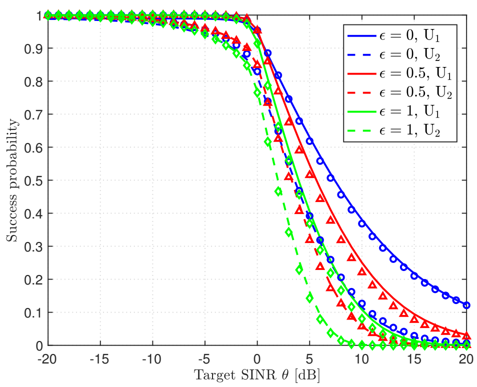

(b) IS$\tilde{\text{I}}$NR-based ordering

Fig. 6. The transmission success probabilities of the NOMA UEs using MSP- and IS$\tilde{\text{I}}$NR-based ordering for $\epsilon \in [0, 1]$ and $N = 2$ in the VD scenario. The curves correspond to the analytical results given in Corollary 2 and Theorem 2 while the markers correspond to the simulation results.

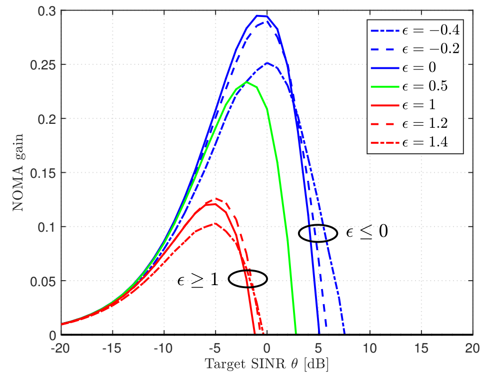

Fig. 7. Simulation results of the NOMA gain for different values of ϵ assuming MSP-based ordering and $N = 2$ for the VD scenario.

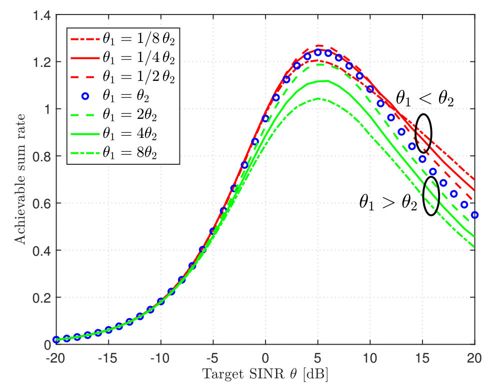

Fig. 8. Analytical results of the achievable sum rate of NOMA with different θ_i for U_i assuming MSP-based ordering, $N = 2$ and $\epsilon = 0$ for the VD scenario. The product $(1 + \theta_1)(1 + \theta_2) = (1 + \theta)^2$ is fixed for all cases to ensure the same target sum rate for the NOMA UEs.

of θ assuming MSP-based ordering. IS$\tilde{\text{I}}$NR-based ordering shows a similar trend except that $\epsilon = 0.5$ exhibits a marginal performance advantage over $\epsilon = 0$ and $\epsilon = 1$ for U_2 when θ is lower than 0 dB.

Fig. 7 depicts the NOMA gain for different ϵ assuming MSP-based ordering and $N = 2$. For a given ϵ, the NOMA gain increases gradually with the increase of θ at first, then starts to sharply decline after reaching the maximum value, and finally drops below zero when θ exceeds a certain threshold, which means that the advantage of NOMA vanishes. For example, for $\epsilon = 1$ (*i.e.,* full power control), NOMA is superior to OMA for $\theta < -1$ dB. For $\epsilon = 0$ (*i.e.,* no power control), NOMA outperforms OMA if θ is below 5 dB. Moreover, the NOMA gain of $\epsilon = 0$ shows a significant advantage over $\epsilon = 1$ for a given θ, which is intuitive based on the results in Fig. 6(a). Furthermore, we consider the case of $\epsilon < 0$ and $\epsilon > 0$ to explore the result if we artificially enhance or overcompensate for the path loss. It is shown that using a negative ϵ improves the NOMA gain for $\theta > 2$ dB. Moreover, the NOMA gain gets more evident for a smaller ϵ given $\epsilon < 0$. The case of $\epsilon = 1.2$ exhibits a marginal improvement of the NOMA gain compared to $\epsilon = 1$ for $\theta > -6$ dB. Further increasing ϵ does not lead to a performance enhancement.

For the VD scenario, we take values of $\theta = -5, 0, 5$ dB and plot the NOMA gain vs. ϵ for the cases of $N = 2$ and $N = 3$. As demonstrated in Fig. 9, there exists an optimal ϵ for each θ to achieve the maximum NOMA gain.[9] Moreover, the optimal value of ϵ decreases as θ increases. For example, for $N = 2$ using IS$\tilde{\text{I}}$NR-based ordering, the optimal value of ϵ for $\theta = 5$ dB is -0.5, which indicates that artificially enhancing the path loss improves the NOMA performance. In comparison, the optimal ϵ is 0.6 for $\theta = -5$ dB, which implies that partial compensation for the path loss results in the optimal performance. Furthermore, the optimal ϵ for IS$\tilde{\text{I}}$NR-based ordering is larger than for MSP-based ordering. Similar conclusions can be drawn for $N = 3$. Moreover, it is shown in Fig. 9 that IS$\tilde{\text{I}}$NR-based ordering is generally superior to MSP-based ordering. Note that the variation of the NOMA gain with respect to ϵ is not completely smooth in Fig. 9, which is due to the fact that the impacts of ϵ on the transmission success probabilities of NOMA UEs are intricate, as shown in (9)-(12) and (17)-(22).

Fig. 8 depicts the achievable sum rate with different θ_i for U_i assuming $N = 2$. The product $(1+\theta_1)(1+\theta_2) = (1+\theta)^2$ is fixed for all cases to ensure the same target sum rate for the NOMA UEs. We observe that setting $\theta_1 > \theta_2$ does not lead

[9]Here we obtain the optimal ϵ for a given N, θ and ordering technique through simulation results. It is rather unlikely that an exact analytical expression of the optimal ϵ that maximizes the NOMA gain can be found. The same applies for Fig. 14.

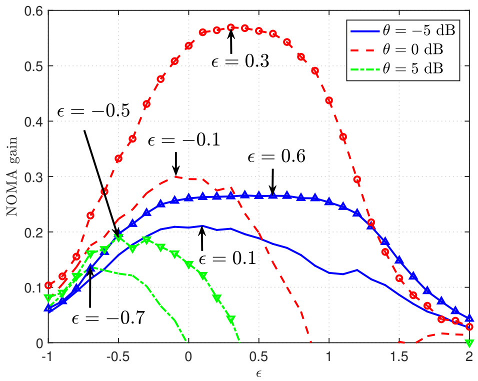

(a) $N = 2$

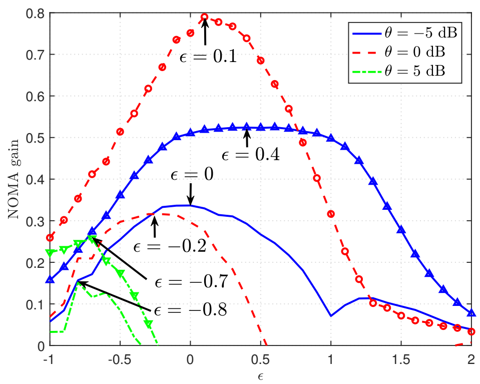

(b) $N = 3$

Fig. 9. Simulation results of the NOMA gain vs. ϵ for $N = 2$ and $N = 3$ in the VD scenario. The markerless curves depict the results for MSP-based ordering while the curves with markers depict the results for IS$\tilde{\text{IN}}$R-based ordering.

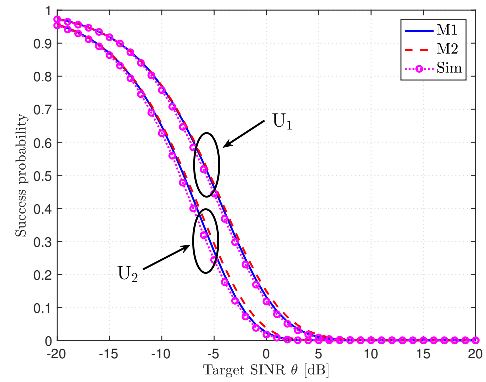

(a) MSP-based

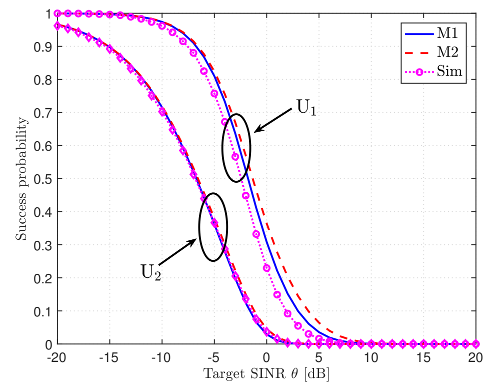

(b) IS$\tilde{\text{IN}}$R-based

Fig. 10. Comparison of the analytical results assuming Model 1 and 2 with the simulation results of the transmission success probabilities of the NOMA UEs for $N = 2$ in the VC scenario. $\lambda = 1$, $\epsilon = 1$, $\alpha = 4$, $\sigma^2 = 0.01$, $\theta_1 = \theta_2 = \theta$ are assumed.

to a performance gain for any value of θ. $\theta_1 = \theta_2$ achieves the optimal performance for $\theta < 2$ dB while $\theta_1 = \frac{1}{2}\theta_2$ leads to the highest sum rate for $\theta \in [2, 10]$ dB. Furthermore, $\theta_1 = \frac{1}{4}\theta_2$ achieves the highest sum rate for $\theta \in [10, 12]$ dB while $\theta_1 = \frac{1}{8}\theta_2$ outperforms the other cases for $\theta > 12$ dB. This indicates that using a smaller rate for U_1 than U_2 leads to a better overall performance in the high-θ regime.

B. The VC Scenario

First, we show that the approximative models of inter-cell interferers we use in the analysis of the VC scenario are sensible. Fig. 10 depicts the analytical results for Model 1 and 2 and the simulation results assuming $N = 2$, $\epsilon = 1$, $\lambda = 1$, $\alpha = 4$, $\sigma^2 = 0.01$ and $\theta_1 = \theta_2 = \theta$. It is shown that the results of Model 1 are lower bounds for Model 2 while both models lead to upper bounds on the simulation results. The analytical and the simulation results match closely for both ordering schemes.

As in Sec. IV-A, we explore the impact of ϵ assuming perfect SIC and the same target SINR for the NOMA UEs. Fig. 11 depicts the transmission success probabilities of U_1 and U_2 using MSP- and IS$\tilde{\text{IN}}$R-based ordering for $\epsilon \in [0, 1]$. It is shown that the performance of both UEs decline with the increase of θ. Moreover, the pace of deterioration accelerates as ϵ increases. Furthermore, it is interesting to find that in the VC scenario, counterintuitively, using power control (*i.e.,* assuming $\epsilon > 0$), which generally reduces signal power disparity between NOMA UEs, does not necessarily degrade the performance. Assuming MSP-based ordering, $\epsilon = 0.5$ results in the best performance for U_1 if θ is lower than -5 dB while $\epsilon = 0$ provides the optimal performance when θ exceeds 5 dB. As for U_2, $\epsilon = 0.5$ results in the best performance for θ lower than 0 dB while $\epsilon = 0$ provides the optimal performance for $\theta > 0$ dB. For the case of IS$\tilde{\text{IN}}$R-based ordering, $\epsilon = 1$, $\epsilon = 0.5$ and $\epsilon = 0$ results in the best performance for U_1 when θ is lower than -10 dB, within $[-10, -2]$ dB, and larger than -2 dB, respectively.

Fig. 12 depicts the NOMA gain for MSP-based ordering assuming $N = 2$. It is shown that the variation of the NOMA gain with respect to θ in the VC scenario exhibits a similar trend as in Fig. 7 for the VD scenario. The advantage of NOMA vanishes when the target SINR exceeds a certain threshold. For example, for $\epsilon = 1$, NOMA is superior to OMA for $\theta < -6$ dB. For $\epsilon = 0$, NOMA outperforms OMA if θ is below 6 dB. Moreover, it is shown that using $\epsilon = -0.5$ leads to the optimal NOMA gain for $\theta > -1$ dB. In contrast, the NOMA gain of $\epsilon = 0$ exceeds all the other cases for $\theta \in [-5, -1]$ dB while $\epsilon = 0.5$ is optimal for $\theta < -5$ dB. Furthermore, we compare the achievable sum rate of NOMA using MSP-based and IS$\tilde{\text{IN}}$R-based ordering for $\epsilon = -0.5, 0, 0.5$. As depicted in Fig. 13, IS$\tilde{\text{IN}}$R-based

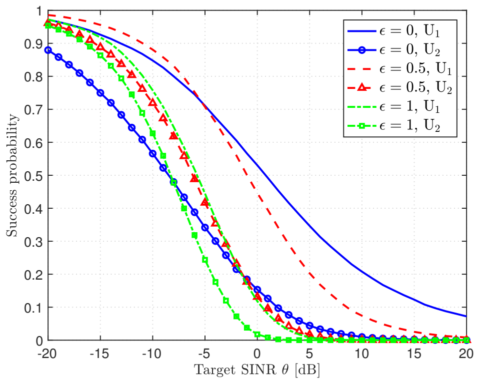

(a) MSP-based

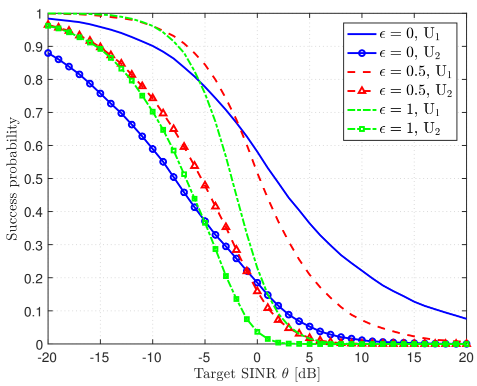

(b) IS$\tilde{\text{I}}$NR-based

Fig. 11. Simulation results of the transmission success probabilities of the NOMA UEs using MSP- and IS$\tilde{\text{I}}$NR-based ordering for $N = 2$ and $\epsilon \in [0, 1]$ in the VC scenario.

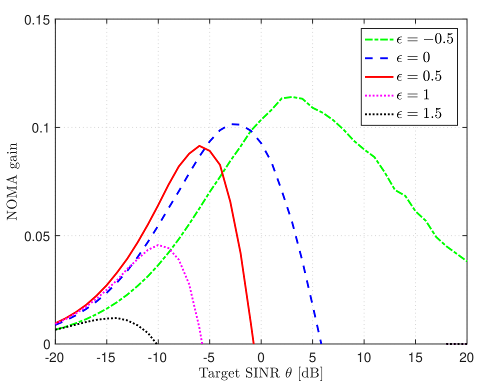

Fig. 12. Simulation results of the NOMA gain for different values of ϵ assuming MSP-based ordering and $N = 2$ for the VC scenario.

ordering is superior to MSP-based ordering for $\epsilon = 0, 0.5$ for all values of θ. However, MSP-based ordering outperforms IS$\tilde{\text{I}}$NR-based ordering as θ exceeds 10 dB for $\epsilon = -0.5$.

For the VC scenario, we also take values of $\theta = -5, 0, 5$ dB and plot the NOMA gain vs. ϵ for the cases of $N = 2$ and $N = 3$. As depicted in Fig. 14, the optimal value of ϵ for IS$\tilde{\text{I}}$NR-based ordering is larger than for MSP-based ordering for $\theta = -5, 0$ dB, which indicates that the NOMA gain improves more for IS$\tilde{\text{I}}$NR-based ordering in response to power control in comparison to MSP-based ordering. In contrast, the optimal ϵ for both ordering schemes are approximately equal for $\theta = 5$ dB. Furthermore, the optimal ϵ decreases as θ increases, which is similar to the observations of the VD scenario in Fig. 9. Based on the comparison of Fig. 9 and Fig. 14, we see that the optimal ϵ for the VD and VC scenarios are close for a given θ and a given ordering scheme, which indicates that the NOMA gain varies in a similar manner in response to power control for the two clustering scenarios.

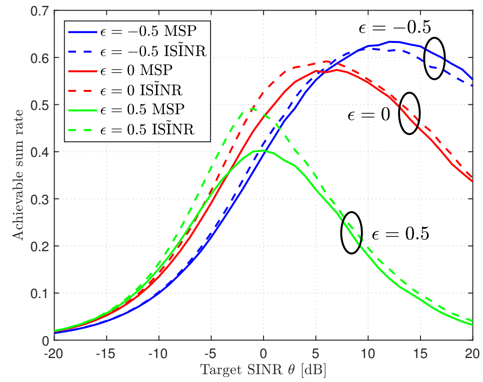

Fig. 13. Analytical results of the achievable sum rate of NOMA with $N = 2$ assuming MSP-based and IS$\tilde{\text{I}}$NR-based ordering for the VC scenario. $\epsilon = -0.5, 0, 0.5$ are assumed.

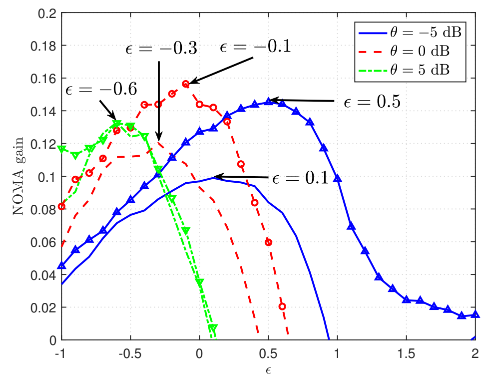

(a) $N = 2$

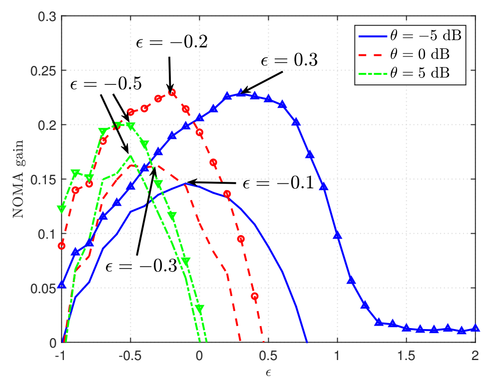

(b) $N = 3$

Fig. 14. Simulation results of the NOMA gain vs. ϵ for $N = 2$ and $N = 3$ in the VC scenario. The markerless curves depict the results for MSP-based ordering while the curves with markers depict the results for IS$\tilde{\text{I}}$NR-based ordering.

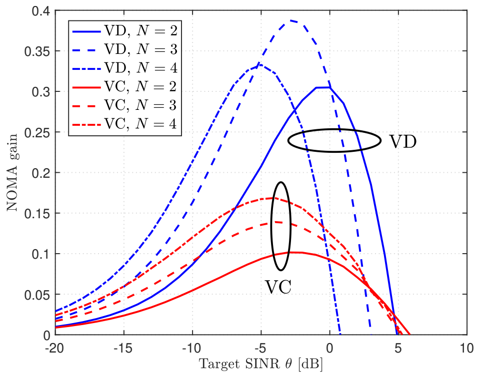

Fig. 15. Simulation results of the NOMA gain of NOMA systems with $N = 2, 3, 4$ and $\epsilon = 0$ assuming MSP-based ordering.

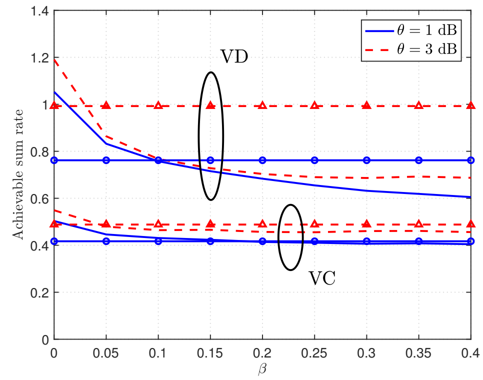

Fig. 16. Analytical results of the achievable sum rate vs. β assuming MSP-based ordering, $N = 2$, $\epsilon = 0$, and the same θ for the NOMA UEs. The markerless curves represent NOMA while the curves with markers represent OMA.

C. Comparison of the VD and VC Scenarios

Fig. 15 depicts a comparison of the NOMA gain for NOMA systems with $N = 2, 3, 4$ under the VD and VC scenarios. $\epsilon = 0$ is selected to obtain the best performance for MSP-based ordering. For the VD scenario, $N = 4$ results in the best performance for $\theta < -5$ dB while $N = 3$ provides the optimal performance for $\theta \in [-5, 0]$ dB. $N = 2$ outweighs $N = 4$ and $N = 3$ for $\theta > 0$ dB. As for the VC scenario, $N = 4$ provides the optimal performance for $\theta < 3$ dB while $N = 2$ provides the optimal performance for $\theta > 3$ dB. Generally, for a given N, the NOMA gain in the VD scenario largely exceeds its counterpart in the VC scenario. Nevertheless, the NOMA gain in the VC scenario is higher than the VD scenario for a relatively large θ, namely 0 dB for $N = 4$ and 3 dB for $N = 3$. However, it is noteworthy that the NOMA gain falls under 0 when θ exceeds 5 dB, which means that NOMA is more beneficial for small θ. Therefore, it can be concluded that the VD clustering scenario is preferable in the application of uplink NOMA in multi-cell scenarios. [13] came to a similar conclusion for downlink NOMA.

We then explore the impact of imperfect SIC on NOMA. Fig. 16 depicts the achievable sum rate vs. β for $\theta = 1, 3$ dB assuming MSP-based ordering, $N = 2$, $\epsilon = 0$, and the same θ for the NOMA UEs. Since OMA does not use SIC, the corresponding sum rate plots are independent of β. The figure shows the existence of a maximum β until which a NOMA system with a particular θ outperforms the corresponding OMA system for both the VD and the VC scenarios. This highlights that a critical minimum level of SIC is required for NOMA to outperform OMA. Moreover, the threshold for the VD scenario is lower than for the VC scenario, which indicates that the VD scenario is more susceptible to the RI. We also observe that the decrease in the sum rate as a function of β is steeper for a larger θ highlighting its increased susceptibility to the RI.

V. Conclusion

In this paper, we have developed a theoretical framework to analyze the performance of multi-cell uplink NOMA systems under two different UE clustering scenarios, namely the VD and VC scenarios. Using some mild simplifying assumptions, we have characterized the Laplace transform of the inter-cell interference with the assumption of fractional power control. Two kinds of UE ordering techniques are analyzed, namely MSP- and IS$\tilde{\text{I}}$NR-based ordering, and the transmission success probabilities of the NOMA UEs taking into account the SIC chain are derived. We show that uplink power control does not necessarily reduce the NOMA performance and identify the selection of the power control exponent given different clustering scenarios and target SINR constraints. Also, we show that IS$\tilde{\text{I}}$NR-based ordering is generally superior to MSP-based ordering. Nevertheless, MSP-based ordering could provide a marginal performance gain over IS$\tilde{\text{I}}$NR-based ordering for large θ if we artificially enhance the path loss, *i.e.,* use negative ϵ, in the VC clustering scenario. Moreover, we show that the advantage of NOMA vanishes when the target SINR exceeds a certain threshold. Furthermore, a critical minimum level of SIC is required for NOMA to outperform OMA.

The results highlight the importance of choosing network parameters such as the power control exponent and the UE ordering technique, depending on the network objective and the target SINR constraint. A comparison of the two UE clustering scenarios indicates that excluding the UEs that are relatively far from the serving BS from the clustering process may improve the NOMA performance.

Appendix A
Proof of Lemma 1

Based on Approximations 1 and 2, the inter-cell interference at the typical BS originating from Φ_{I} is given as

$$\begin{aligned} I^{\star} &\approx \sum_{\substack{y\in\Phi \\ \|y\|>\rho}} \sum_{i=1}^{N} P_{i,y} h_{i,y} \|y\|^{-\alpha} + \sum_{\substack{y\in\Phi \\ \|y\|=\rho}} \sum_{i=1}^{N} P_{i,y} h_{i,y} \|y\|^{-\alpha} \\ &= \underbrace{\sum_{\substack{y\in\Phi \\ \|y\|>\rho}} \sum_{i=1}^{N} R_{i,y}^{\alpha\epsilon} h_{i,y} \|y\|^{-\alpha}}_{I_{\mathrm{nn}}^{\star}} + \underbrace{\sum_{i=1}^{N} R_{i,y_\rho}^{\alpha\epsilon} h_{i,y_\rho} \rho^{-\alpha}}_{I_{\mathrm{n}}^{\star}}, \end{aligned} \tag{42}$$

where $I^\star_{\rm nn}$ denotes the inter-cell interference which originates from UEs in the non-neareast cells while $I^\star_{\rm n}$ denotes the interference that stems from UEs in the neareast cell[10].

The LT of $I^\star$ given ρ is thus given as

$$\mathcal{L}_{I^\star|\rho}(s) \approx \mathcal{L}_{I^\star_{\rm nn}|\rho}(s)\cdot\mathcal{L}_{I^\star_{\rm n}|\rho}(s). \tag{43}$$

$\mathcal{L}_{I^\star_{\rm nn}|\rho}(s)$ is obtained as

$$\begin{aligned}
\mathcal{L}_{I^\star_{\rm nn}|\rho}(s) &= \mathbb{E}\Big[\exp\Big(-s\sum_{\substack{y\in\Phi\\ \|y\|>\rho}}\sum_{i=1}^{N}R_{i,y}^{\alpha\epsilon}h_{i,y}\|y\|^{-\alpha}\Big)\Big]\\
&\overset{(a)}{=} \mathbb{E}_\Phi\Big[\prod_{\substack{y\in\Phi\\ \|y\|>\rho}}\mathbb{E}_{R_{i,y}}\Big[\prod_{i=1}^{N}\frac{1}{1+sR_{i,y}^{\alpha\epsilon}\|y\|^{-\alpha}}\Big]\Big]\\
&\overset{(b)}{=} \mathbb{E}_\Phi\Big[\prod_{\substack{y\in\Phi\\ \|y\|>\rho}}\Big(\int_0^{\frac{\rho}{2}}\frac{f_{R_{i,y}|\rho}(x)}{1+sx^{\alpha\epsilon}\|y\|^{-\alpha}}\mathrm{d}x\Big)^N\Big]\\
&\overset{(c)}{=} \exp\Big(-2\pi\lambda\int_\rho^\infty\Big(1-\Big(\underbrace{\int_0^{\frac{\rho}{2}}\frac{f_{R_{i,y}|\rho}(x)}{1+sx^{\alpha\epsilon}y^{-\alpha}}\mathrm{d}x}_{A}\Big)^N\Big)y\mathrm{d}y\Big),
\end{aligned} \tag{44}$$

where (a) follows from $h_{i,y}\sim\exp(1)$ and the independence between $h_{i,y}$, (b) follows since $R_{i,y}$ are i.i.d. for $1\le i\le N$, (c) follows from mapping Φ to one dimension and applying the probability generating functional (pgfl) of the PPP [20].

The integral A is calculated as

$$\begin{aligned}
A &= \int_0^{\frac{\rho}{2}}\frac{1}{1+sx^{\alpha\epsilon}y^{-\alpha}}\frac{8x}{\rho^2}\mathrm{d}x\\
&\overset{(d)}{=} \frac{4\delta}{\epsilon\rho^2}\int_0^{(\frac{\rho}{2})^{\alpha\epsilon}}\frac{u^{\frac{\delta}{\epsilon}-1}}{1+sy^{-\alpha}u}\mathrm{d}u\\
&\overset{(e)}{=} {}_2F_1\Big(1,\frac{\delta}{\epsilon};1+\frac{\delta}{\epsilon};-s\Big(\frac{\rho}{2}\Big)^{\alpha\epsilon}y^{-\alpha}\Big),
\end{aligned} \tag{45}$$

where (d) follows from the substitution $u=x^{\alpha\epsilon}$, $\delta=\frac{2}{\alpha}$ and $\epsilon\ne0$, (e) follows from $\epsilon>0$ and $\int_0^t\frac{x^{\mu-1}}{(1+\beta x)^v}\mathrm{d}x = \frac{t^\mu}{\mu}{}_2F_1(v,\mu;1+\mu;-\beta t), \mu>0$ [23, Eqn. 3.194.1].

$\mathcal{L}_{I^\star_{\rm n}|\rho}(s)$ is obtained as

$$\begin{aligned}
\mathcal{L}_{I^\star_{\rm n}|\rho}(s) &= \mathbb{E}\Big[\exp\Big(-s\sum_{i=1}^{N}R_{i,y_\rho}^{\alpha\epsilon}h_{i,y_\rho}\rho^{-\alpha}\Big)\Big]\\
&\overset{(f)}{=} \Big(\int_0^{\frac{\rho}{2}}\frac{f_{R_{i,y_\rho}|\rho}(x)}{1+sx^{\alpha\epsilon}\rho^{-\alpha}}\mathrm{d}x\Big)^N\\
&\overset{(g)}{=} \Big({}_2F_1\Big(1,\frac{\delta}{\epsilon};1+\frac{\delta}{\epsilon};-s\Big(\frac{\rho}{2}\Big)^{\alpha\epsilon}\rho^{-\alpha}\Big)\Big)^N,
\end{aligned} \tag{46}$$

where (f) follows since $h_{i,y_\rho}\sim\exp(1)$, h_{i,y_ρ} are i.i.d. and $R_{i,y}$ are i.i.d., (g) follows from (45) by replacing y with ρ.

Combining (46) and (44), we obtain (3).

[10]The nearest cell refers to the cell whose serving BS is the nearest neighbor of the typical BS. The other interfering cells are referred to as the non-nearest cells. In (42), we denote the location of the nearest BS, which is at distance ρ from the typical BS, as y_ρ.

Appendix B
Proof of Corollary 1

Assuming that the interfering UEs use transmit power $\bar{P}$, the LT of $I^\star_{\rm nn}$ is approximated as

$$\begin{aligned}
\mathcal{L}_{I^\star_{\rm nn}|\rho}(s) &\approx \exp\Big(-2\pi\lambda\int_\rho^\infty\Big(1-\Big(\frac{1}{1+s\bar{P}y^{-\alpha}}\Big)^N\Big)y\mathrm{d}y\Big)\\
&\overset{(a)}{=} \exp\Big(-\pi\lambda\delta\int_0^{\rho^{-\alpha}}\Big(1-\Big(1-\frac{s\bar{P}u}{1+s\bar{P}u}\Big)^N\Big)u^{-\delta-1}\mathrm{d}u\Big)\\
&\overset{(b)}{=} \exp\Big(-\pi\lambda\delta\sum_{k=1}^{N}\binom{N}{k}(-1)^{k+1}s^k\bar{P}^k\int_0^{\rho^{-\alpha}}\frac{u^{k-\delta-1}}{(1+s\bar{P}u)^k}\mathrm{d}u\Big)\\
&\overset{(c)}{=} \exp\Big(-\sum_{k=1}^{N}\binom{N}{k}W_k(\rho)s^k{}_2F_1\Big(k,k-\delta;k+1-\delta;-\frac{s\bar{P}}{\rho^\alpha}\Big)\Big),
\end{aligned} \tag{47}$$

where (a) follows from the substitution $u=y^{-\alpha}$ and $\delta=2/\alpha$, (b) follows from the binomial expansion of $\Big(1-\frac{s\bar{P}u}{1+s\bar{P}u}\Big)^N$, and (c) follows from [23, Eqn. 3.194.1].

$\mathcal{L}_{I^\star_{\rm n}|\rho}(s)$ is approximated as

$$\mathcal{L}_{I^\star_{\rm n}|\rho}(s) \approx \mathbb{E}\Big[\exp\Big(-s\sum_{i=1}^{N}\bar{P}h_{i,y_\rho}\rho^{-\alpha}\Big)\Big] = \frac{1}{(1+s\bar{P}\rho^{-\alpha})^N}. \tag{48}$$

Combining (47) and (48), we obtain (6).

Appendix C
Proof of Theorem 1

Assuming $\epsilon\le1$,

$$\begin{aligned}
\mathbb{P}(C_i) &= \mathbb{P}\Bigg[\frac{h_1\hat{R}_1^{-(1-\epsilon)\alpha}}{\sum_{j=2}^{N}h_j\hat{R}_j^{-(1-\epsilon)\alpha}+I^\star+\sigma^2}>\theta_1,...,\\
&\qquad \frac{h_i\hat{R}_i^{-(1-\epsilon)\alpha}}{\sum_{j=i+1}^{N}h_j\hat{R}_j^{-(1-\epsilon)\alpha}+I^\star+\sigma^2}>\theta_i\Bigg]\\
&\overset{(a)}{=} \mathbb{E}\Bigg[\int_0^\infty\mathrm{d}h_N\cdots\int_0^\infty\mathrm{d}h_{i+1}\int_{\theta_i(\sum_{j=i+1}^{N}h_j\hat{R}_j^{-(1-\epsilon)\alpha}+I^\star+\sigma^2)}^\infty\mathrm{d}h_i\\
&\qquad\times\cdots\times\int_{\theta_1(\sum_{j=2}^{N}h_j\hat{R}_j^{-(1-\epsilon)\alpha}+I^\star+\sigma^2)}^\infty\mathrm{d}h_1e^{-h_1}\cdots e^{-h_N}\Bigg],\\
&= \mathbb{E}\Bigg[\prod_{k=1}^{i}a_k\prod_{j=i+1}^{N}b_{i,j}e^{-(I^\star+\sigma^2)d_i}\Bigg],
\end{aligned} \tag{49}$$

where (a) follows from $h_i\sim\exp(1)$ and the independence between h_i for $1\le i\le N$. Applying the definition of the Laplace transform, we obtain (9).

For $\epsilon>1$,

$$\begin{aligned}
\mathbb{P}(C_i) &= \mathbb{P}\Bigg[\frac{h_N\hat{R}_N^{-(1-\epsilon)\alpha}}{\sum_{j=1}^{N-1}h_j\hat{R}_j^{-(1-\epsilon)\alpha}+I^\star+\sigma^2}>\theta_1,...,\\
&\qquad \frac{h_{N+1-i}\hat{R}_{N+1-i}^{-(1-\epsilon)\alpha}}{\sum_{j=1}^{N-i}h_j\hat{R}_j^{-(1-\epsilon)\alpha}+I^\star+\sigma^2}>\theta_i\Bigg].
\end{aligned} \tag{50}$$

Following similar derivations as in (49), we obtain (9).

Appendix D
Proof of Corollary 2

Define

$$E(\rho, r_1) \triangleq \int_{r_1}^{\frac{\rho}{2}} \frac{f_{R_2}(r_2)}{1+\theta_1 r_1^{(1-\epsilon)\alpha} r_2^{-(1-\epsilon)\alpha}} \mathrm{d}r_2$$
$$\stackrel{(a)}{=} \frac{4\delta_\epsilon}{\rho^2} \int_{(\frac{\rho}{2})^{-\frac{2}{\delta_\epsilon}}}^{r_1^{-\frac{2}{\delta_\epsilon}}} \frac{v^{-\delta_\epsilon - 1}}{1+\theta_1 r_1^{\frac{2}{\delta_\epsilon}} v} \mathrm{d}v = \frac{4\delta_\epsilon}{\rho^2} T_\epsilon(\rho, r_1), \tag{51}$$

where (a) follows from the substitution $v = r_2^{-(1-\epsilon)\alpha}$ and $\delta_\epsilon = \frac{2}{(1-\epsilon)\alpha}$.

Assuming $\epsilon < 1$, from (9) we have

$$\mathbb{P}(C_1) = \mathbb{E}_\rho\left[\mathbb{E}_{\hat{R}_1,\hat{R}_2}\left[\frac{e^{-\theta_1\sigma^2\hat{R}_1^{(1-\epsilon)\alpha}}\mathcal{L}_{I^\star|\rho}(\theta_1\hat{R}_1^{(1-\epsilon)\alpha})}{1+\theta_1\hat{R}_1^{(1-\epsilon)\alpha}\hat{R}_2^{-(1-\epsilon)\alpha}}\right]\right]$$
$$\stackrel{(b)}{=} \mathbb{E}_\rho\left[\int_0^{\frac{\rho}{2}} 2e^{-\theta_1\sigma^2 r_1^{(1-\epsilon)\alpha}}\mathcal{L}_{I^\star|\rho}(\theta_1 r_1^{(1-\epsilon)\alpha}) f_{R_1}(r_1) E(\rho, r_1)\mathrm{d}r_1\right], \tag{52}$$

where (b) follows from $f_{\hat{R}_1,\hat{R}_2}(r_1,r_2) = 2f_{R_1}(r_1)f_{R_2}(r_2)$ based on order statistics [22]. Substituting (51) in (52), we get (13). Similarly,

$$\mathbb{P}(C_2) = \mathbb{E}_\rho\left[\mathbb{E}_{\hat{R}_1,\hat{R}_2}\left[\frac{e^{-\sigma^2 v_\epsilon(\hat{R}_1,\hat{R}_2)}\mathcal{L}_{I^\star|\rho}(v_\epsilon(\hat{R}_1,\hat{R}_2))}{1+\theta_1\hat{R}_1^{(1-\epsilon)\alpha}\hat{R}_2^{-(1-\epsilon)\alpha}}\right]\right]. \tag{53}$$

Applying the joint pdf of $\hat{R}_1$ and $\hat{R}_2$ and some simplifications, we obtain (15). Using similar derivations, we obtain the results for $\epsilon > 1$ and $\epsilon = 1$ as given in (13) and (15).

Appendix E
Impact of imperfect SIC

Considering imperfect SIC, the SINR of U_i for $1 \le i \le N$ is

$$\mathrm{SINR}_i = \frac{h_i R_i^{-(1-\epsilon)\alpha}}{\sum_{j=i+1}^{N} h_j R_j^{-(1-\epsilon)\alpha} + \beta\sum_{q=1}^{i-1} h_q R_q^{-(1-\epsilon)\alpha} + I^\star + \sigma^2}, \tag{54}$$

where $\beta \in [0,1]$ is the fraction of residual interference (RI) from UEs decoded before U_i. $\beta = 0$ means perfect SIC, while $\beta = 1$ corresponds to no SIC at all. Using similar derivations as in the perfect SIC case, the transmission success probabilities of the NOMA UEs can be derived. As an example, here we give the expression of $\mathbb{P}(C_2)$ considering imperfect SIC using MSP-based ordering for the VD scenario with $N = 2$. $\mathbb{P}(C_2)$ is given in (55) for $\theta_1\theta_2\beta < 1$, where

$$w_\epsilon(r_1,r_2) = \frac{1}{1+\theta_1 r_1^{2/\delta_\epsilon} r_2^{-2/\delta_\epsilon}} - \frac{1}{1+\theta_2^{-1}\beta^{-1} r_1^{2/\delta_\epsilon} r_2^{-2/\delta_\epsilon}}, \tag{56}$$

$$u_\epsilon(r_1,r_2) = \frac{\theta_1(1+\theta_2)}{1-\theta_1\theta_2\beta} r_1^{2/\delta_\epsilon} + \frac{\theta_2(1+\theta_1\beta)}{1-\theta_1\theta_2\beta} r_2^{2/\delta_\epsilon}. \tag{57}$$

For $\theta_1\theta_2\beta \ge 1$, $\mathbb{P}(C_2) = 0$. The numerical results are given in Fig. 16.

Appendix F
Proof of Theorem 2

For $\theta \ge 1$,

$$\mathbb{P}(C_1) = \mathbb{P}\left[\hat{Z}_1 > \theta\hat{Z}_2 + \theta \mid \hat{Z}_1 > \hat{Z}_2\right] = \mathbb{P}\left[\hat{Z}_1 > \theta\hat{Z}_2 + \theta\right]$$
$$= \mathbb{E}_{\rho,R_1,R_2}\left[\int_0^\infty \int_{\theta z_2+\theta}^\infty f_{\hat{Z}_1,\hat{Z}_2|\rho,R_1,R_2}(z_1,z_2)\mathrm{d}z_1\mathrm{d}z_2\right]$$
$$\stackrel{(a)}{=} \mathbb{E}_{\rho,R_1,R_2}\left[\int_0^\infty \int_{\theta z_2+\theta}^\infty 2f_{Z_1|\rho,R_1}(z_1) f_{Z_2|\rho,R_2}(z_2)\mathrm{d}z_1\mathrm{d}z_2\right], \tag{58}$$

where (a) follows from $f_{\hat{Z}_1,\hat{Z}_2|\rho,R_1,R_2}(z_1,z_2) = 2f_{Z_1|\rho,R_1}(z_1)f_{Z_2|\rho,R_2}$ based on order statistics [22].

The cumulative distribution function (cdf) of the unordered Z_i conditioned on ρ and R_i is given as[11]

$$F_{Z_i|\rho,R_i}(z) = \mathbb{P}\left[\frac{h_i R_i^{-(1-\epsilon)\alpha}}{I^\star + \sigma^2} < z\right]$$
$$\stackrel{(b)}{=} 1 - e^{-z\sigma^2 R_i^{(1-\epsilon)\alpha}}\mathcal{L}_{I^\star|\rho}(zR_i^{(1-\epsilon)\alpha}), \tag{59}$$

where (b) follows from $h_i \sim \exp(1)$ and the definition of the LT. The conditional pdf of Z_i is thus obtained as

$$f_{Z_i|\rho,R_i}(z) = \frac{\mathrm{d}F_{Z_i|\rho,R_i}(z)}{\mathrm{d}z}$$
$$= R_i^{(1-\epsilon)\alpha} e^{-z\sigma^2 R_i^{(1-\epsilon)\alpha}}\left(\sigma^2\mathcal{L}_{I^\star|\rho}(zR_i^{(1-\epsilon)\alpha}) - \mathcal{L}'_{I^\star|\rho}(zR_i^{(1-\epsilon)\alpha})\right), \tag{60}$$

where $\mathcal{L}'_{I^\star|x}(s) = \mathrm{d}\mathcal{L}_{I^\star|x}(s)/\mathrm{d}s$ can be obtained from (6). Substituting (60) in (58), we get the results in (17).

For $\theta < 1$, we have

$$\mathbb{P}(C_1) = \mathbb{P}\left[\hat{Z}_1 > \theta\hat{Z}_2 + \theta, 0 \le \hat{Z}_2 \le \frac{\theta}{1-\theta}\right] + \mathbb{P}\left[\hat{Z}_1 > \hat{Z}_2, \hat{Z}_2 > \frac{\theta}{1-\theta}\right]. \tag{61}$$

Using similar derivations, we obtain (19). Similarly, we can obtain the results for U_2.

[11] The unordered Z_i are independent for $i = 1, 2$.

$$\mathbb{P}(C_2) = \begin{cases} \int_0^\infty \int_0^{\frac{x}{2}} \int_{r_1}^{\frac{x}{2}} w_\epsilon(r_1,r_2) e^{-\sigma^2 u_\epsilon(r_1,r_2)}\mathcal{L}_{I^\star|\rho}(u_\epsilon(r_1,r_2))\mathrm{d}r_2\mathrm{d}r_1 f_\rho(x)\mathrm{d}x, & \epsilon < 1, \\ \int_0^\infty \int_0^{\frac{x}{2}} \int_0^{r_2} w_\epsilon(r_2,r_1) e^{-\sigma^2 u_\epsilon(r_2,r_1)}\mathcal{L}_{I^\star|\rho}(u_\epsilon(r_2,r_1))\mathrm{d}r_1\mathrm{d}r_2 f_\rho(x)\mathrm{d}x, & \epsilon > 1, \\ \frac{1-\theta_1\theta_2\beta}{(1+\theta_1)(1+\theta_2\beta)} e^{-\frac{\theta_2+\theta_1(1+\theta_2+\theta_2\beta)}{1-\theta_1\theta_2\beta}\sigma^2} \int_0^\infty \mathcal{L}_{I^\star|\rho}\Big(\frac{\theta_2+\theta_1(1+\theta_2+\theta_2\beta)}{1-\theta_1\theta_2\beta}\Big) f_\rho(x)\mathrm{d}x, & \epsilon = 1, \end{cases} \tag{55}$$

Appendix G
Proof of Lemma 2

For Model 1, the inter-cell interference at the typical BS originating from $\Psi_{\rm I}$ is denoted as I^* and given by

$$I^* = \sum_{x\in\Psi_{\rm I}} P_x h_x \|x\|^{-\alpha} = \sum_{x\in\Psi_{\rm I}} R_x^{\alpha\epsilon} h_x D_x^{-\alpha}. \tag{62}$$

The LT of I^* is given as

$$\begin{aligned}
&\mathcal{L}_{I^*}(s) = \mathbb{E}\Big[\exp\Big(-s\sum_{x\in\Psi_{\rm I}} R_x^{\alpha\epsilon} h_x D_x^{-\alpha}\Big)\Big] \\
&\stackrel{(a)}{=} \mathbb{E}_{\Psi_{\rm I}}\Big[\prod_{x\in\Psi_{\rm I}} \mathbb{E}_{R_x}\left[\frac{1}{1+sR_x^{\alpha\epsilon}D_x^{-\alpha}}|D_x\right]\Big] \\
&\stackrel{(b)}{=} \mathbb{E}_{\Psi_{\rm I}}\Big[\prod_{x\in\Psi_{\rm I}} \int_0^{D_x} \frac{2a\pi\lambda y e^{-a\pi\lambda y^2}}{(1-e^{-a\pi\lambda D_x^2})(1+sy^{\alpha\epsilon}D_x^{-\alpha})}{\rm d}y\Big] \\
&\stackrel{(c)}{=} \exp\Big(-2\pi N\lambda\int_0^\infty\left(1-e^{-b\pi\lambda z^2}\right)(1-\mu_1(z,s))z{\rm d}z\Big),
\end{aligned} \tag{63}$$

where (a) follows from $h_x\sim\exp(1)$ and the independence between h_x, (b) uses (26) to average over R_x, (c) follows from (27), applying the pgfl of the general PPP [20], mapping $\Psi_{\rm I}$ to one dimension, and the substitution $\mu_n(z,s) = \int_0^z \frac{2a\pi\lambda y e^{-a\pi\lambda y^2}}{(1-e^{-a\pi\lambda z^2})(1+sy^{\varepsilon\alpha}z^{-\alpha})^n}{\rm d}y$.

For Model 2, the LT of the inter-cell interference at the typical BS is given as

$$\mathcal{L}_{I^*}(s) = \mathbb{E}\Big[\exp\Big(-s\sum_{x\in\Psi_{\rm p}}\sum_{i=1}^{N} R_x^{\alpha\epsilon} h_{x,i} D_x^{-\alpha}\Big)\Big]. \tag{64}$$

Using similar derivations as in (63), we obtain (29).

Appendix H
Proof of Corollary 3

Define

$$\begin{aligned}
F(r_1) &\triangleq \int_{r_1}^\infty \frac{f_{R_2}(r_2)}{1+\theta_1 r_1^{(1-\epsilon)\alpha} r_2^{-(1-\epsilon)\alpha}}{\rm d}r_2 \\
&= \int_{r_1}^\infty \frac{2a\pi\lambda x e^{-a\pi\lambda x^2}}{1+\theta_1 r_1^{(1-\epsilon)\alpha}x^{-(1-\epsilon)\alpha}}{\rm d}x \\
&\stackrel{(a)}{=} \delta_\epsilon a\pi\lambda r_1^2\int_0^1 \frac{v^{-\delta_\epsilon-1}e^{-a\pi\lambda r_1^2 v^{-\delta_\epsilon}}}{1+\theta_1 v}{\rm d}v \\
&= \xi_{\delta_\epsilon}(a\pi\lambda r_1^2,\theta_1),
\end{aligned} \tag{65}$$

where (a) follows from the substitution $v=(\frac{x}{r_1})^{-(1-\epsilon)\alpha}$ and $\delta_\epsilon = \frac{2}{(1-\epsilon)\alpha}$.

Assuming $\epsilon<1$, from (31) we have

$$\begin{aligned}
&\mathbb{P}(C_1) = \mathbb{P}\left[\frac{h_1\hat{R}_1^{-(1-\epsilon)\alpha}}{h_2\hat{R}_2^{-(1-\epsilon)\alpha}+I^*+\sigma^2} > \theta_1\right] \\
&\stackrel{(b)}{=} \mathbb{E}_{\hat{R}_1,\hat{R}_2}\left[\frac{e^{-\theta_1\sigma^2\hat{R}_1^{(1-\epsilon)\alpha}}\mathcal{L}_{I^*}(\theta_1\hat{R}_1^{(1-\epsilon)\alpha})}{1+\theta_1\hat{R}_1^{(1-\epsilon)\alpha}\hat{R}_2^{-(1-\epsilon)\alpha}}\right] \\
&\stackrel{(c)}{=} \int_0^\infty 2e^{-\theta_1\sigma^2 r_1^{(1-\epsilon)\alpha}}\mathcal{L}_{I^*}(\theta_1 r_1^{(1-\epsilon)\alpha})F(r_1)f_{R_1}(r_1){\rm d}r_1,
\end{aligned} \tag{66}$$

where (b) follows from $h_1\sim\exp(1), h_2\sim\exp(1)$ and the independence of h_1 and h_2, (c) follows from $f_{\hat{R}_1,\hat{R}_2}(r_1,r_2) = 2f_{R_1}(r_1)f_{R_2}(r_2)$ based on order statistics [22]. Substituting (65) in (66), we get (32). Similarly,

$$\begin{aligned}
&\mathbb{P}(C_2) = \mathbb{P}\left[\frac{h_1\hat{R}_1^{-(1-\epsilon)\alpha}}{h_2\hat{R}_2^{-(1-\epsilon)\alpha}+I^*+\sigma^2} > \theta_1, \frac{h_2\hat{R}_2^{-(1-\epsilon)\alpha}}{I^*+\sigma^2} > \theta_2\right] \\
&\stackrel{(d)}{=} \mathbb{E}_{\hat{R}_1,\hat{R}_2}\left[\frac{e^{-\sigma^2 v_\epsilon(\hat{R}_1,\hat{R}_2)}\mathcal{L}_{I^*}(v_\epsilon(\hat{R}_1,\hat{R}_2))}{1+\theta_1\hat{R}_1^{(1-\epsilon)\alpha}\hat{R}_2^{-(1-\epsilon)\alpha}}\right],
\end{aligned} \tag{67}$$

where (d) follows from $h_1\sim\exp(1), h_2\sim\exp(1)$ and the independence of h_1 and h_2. Applying the joint pdf of $\hat{R}_1$ and $\hat{R}_2$ and some simplifications, we get (34). Using similar derivations, we obtain the results for $\epsilon>1$ and $\epsilon=1$ as given in (32) and (34).

Appendix I
Proof of Theorem 4

For $\theta_1\geq 1$,

$$\begin{aligned}
&\mathbb{P}(C_1) = \mathbb{P}\left[\hat{Z}_1 > \theta_1\hat{Z}_2+\theta_1\right] \\
&\stackrel{(a)}{=} \mathbb{E}_{R_1,R_2}\left[\int_0^\infty\int_{\theta_1 z_2+\theta_1}^\infty 2f_{Z_1|R_1}(z_1)f_{Z_2|R_2}(z_2){\rm d}z_1{\rm d}z_2\right],
\end{aligned} \tag{68}$$

where (a) follows from $f_{\hat{Z}_1,\hat{Z}_2|R_1,R_2}(z_1,z_2) = 2f_{Z_1|R_1}(z_1)f_{Z_2|R_2}(z_2)$ based on order statistics.

The cdf of the unordered Z_i conditioned on R_i is given as

$$\begin{aligned}
F_{Z_i|R_i}(z) &= \mathbb{P}\Big[\frac{h_iR_i^{-(1-\epsilon)\alpha}}{I^*+\sigma^2} < z\Big] \\
&\stackrel{(b)}{=} 1-\exp(-z\sigma^2R_i^{\frac{2}{\delta_\epsilon}})\mathcal{L}_{I^*}(zR_i^{\frac{2}{\delta_\epsilon}}),
\end{aligned} \tag{69}$$

where (b) follows from $h_i\sim\exp(1)$ and the definition of the LT. The conditional pdf of Z_i is thus obtained as

$$\begin{aligned}
f_{Z_i|R_i}(z) &= \frac{{\rm d}F_{Z_i|R_i}(z)}{{\rm d}z} \\
&= R_i^{\frac{2}{\delta_\epsilon}}\exp(-z\sigma^2R_i^{\frac{2}{\delta_\epsilon}})\Big(\sigma^2\mathcal{L}_{I^*}(zR_i^{\frac{2}{\delta_\epsilon}}) - \mathcal{L}'_{I^*}(zR_i^{\frac{2}{\delta_\epsilon}})\Big),
\end{aligned} \tag{70}$$

where $\mathcal{L}'_{I^*}(s) = {\rm d}\mathcal{L}_{I^*}(s)/{\rm d}s$ can be obtained from (28) and (29). Substituting (70) in (68), we get (35).

For $\theta_1<1$, we have

$$\begin{aligned}
\mathbb{P}(C_1) =& \mathbb{P}\left[\hat{Z}_1 > \theta_1\hat{Z}_2+\theta_1, 0\leq\hat{Z}_2\leq\frac{\theta_1}{1-\theta_1}\right] \\
&+\mathbb{P}\left[\hat{Z}_1>\hat{Z}_2, \hat{Z}_2>\frac{\theta_1}{1-\theta_1}\right].
\end{aligned} \tag{71}$$

Using similar derivations, we obtain (37). Similarly, we can obtain the results for $\rm U_2$.

References

[1] *Evolved Universal Terrestrial Radio Access (E-UTRA); Overall description; Stage 2*, 3GPP TS 36.300 V13.2.0, Jan. 2016.

[2] J. G. Andrews, S. Buzzi, W. Choi, S. V. Hanly, A. Lozano, A. C. Soong, and J. C. Zhang, "What will 5G be?" *IEEE J. Sel. Areas Commun.*, vol. 32, no. 6, pp. 1065–1082, Jun. 2014.

[3] S. Vanka, S. Srinivasa, Z. Gong, P. Vizi, K. Stamatiou, and M. Haenggi, "Superposition coding strategies: Design and experimental evaluation," *IEEE Trans. Wireless Commun.*, vol. 11, no. 7, pp. 2628–2639, Jul. 2012.

[4] Y. Saito, Y. Kishiyama, A. Benjebbour, T. Nakamura, A. Li, and K. Higuchi, "Non-orthogonal multiple access (NOMA)

for cellular future radio access," in *2013 IEEE 77th Vehicular Technology Conference (VTC Spring)*, Jun. 2013, pp. 1–5.
[5] Z. Ding, Z. Yang, P. Fan, and H. V. Poor, "On the performance of non-orthogonal multiple access in 5G systems with randomly deployed users," *IEEE Signal Process. Lett.*, vol. 21, no. 12, pp. 1501–1505, Dec. 2014.
[6] Z. Ding, P. Fan, and H. V. Poor, "Impact of user pairing on 5G nonorthogonal multiple-access downlink transmissions," *IEEE Trans. Veh. Technol.*, vol. 65, no. 8, pp. 6010–6023, Aug. 2016.
[7] Z. Yang, Z. Ding, P. Fan, and N. Al-Dhahir, "A general power allocation scheme to guarantee quality of service in downlink and uplink NOMA systems," *IEEE Trans. Wireless Commun.*, vol. 15, no. 11, pp. 7244–7257, Aug. 2016.
[8] N. Zhang, J. Wang, G. Kang, and Y. Liu, "Uplink nonorthogonal multiple access in 5G systems," *IEEE Commun. Lett.*, vol. 20, no. 3, pp. 458–461, Mar. 2016.
[9] Y. Liu, M. Derakhshani, and S. Lambotharan, "Outage analysis and power allocation in uplink non-orthogonal multiple access systems," *IEEE Commun. Lett.*, vol. 22, no. 2, pp. 336–339, Feb. 2018.
[10] Z. Zhang, H. Sun, and R. Q. Hu, "Downlink and uplink non-orthogonal multiple access in a dense wireless network," *IEEE J. Sel. Areas Commun.*, vol. 35, no. 12, pp. 2771–2784, Jul. 2017.
[11] K. S. Ali, M. Haenggi, H. ElSawy, A. Chaaban, and M.-S. Alouini, "Downlink non-orthogonal multiple access (NOMA) in Poisson networks," *IEEE Trans. Commun.*, vol. 67, no. 2, pp. 1613–1628, Feb. 2019.
[12] K. S. Ali, H. ElSawy, A. Chaaban, M. Haenggi, and M.-S. Alouini, "Analyzing non-orthogonal multiple access (NOMA) in downlink Poisson cellular networks," in *Proc. of IEEE International Conference on Communications (ICC18)*, May 2018, pp. 1–5.
[13] K. S. Ali, H. ElSawy, and M.-S. Alouini, "Meta distribution of downlink non-orthogonal multiple access (NOMA) in Poisson networks," *IEEE Wireless Commun. Lett.*, vol. 8, no. 2, pp. 572–575, Apr. 2019.
[14] M. Salehi, H. Tabassum, and E. Hossain, "Meta distribution of the SIR in large-scale uplink and downlink NOMA networks," *IEEE Trans. Commun.*, vol. 67, no. 4, pp. 3009–3025, Apr. 2019.
[15] H. Tabassum, E. Hossain, and J. Hossain, "Modeling and analysis of uplink non-orthogonal multiple access in large-scale cellular networks using Poisson cluster processes," *IEEE Trans. Commun.*, vol. 65, no. 8, pp. 3555–3570, Apr. 2017.
[16] M. Haenggi, "User point processes in cellular networks," *IEEE Wireless Commun. Lett.*, vol. 6, no. 2, pp. 258–261, Apr. 2017.
[17] ——, "The meta distribution of the SIR in Poisson bipolar and cellular networks," *IEEE Trans. Wireless Commun.*, vol. 15, no. 4, pp. 2577–2589, Apr. 2016.
[18] *Evolved Universal Terrestrial Radio Access (E-UTRA); Physical layer procedures*, 3GPP TR36.213 V12.4.0, Dec. 2014.
[19] M. Salehi, H. Tabassum, and E. Hossain, "Accuracy of distance-based ranking of users in the analysis of NOMA systems," *IEEE Trans. Commun.*, vol. 67, no. 7, pp. 5069–5083, Jul. 2019.
[20] M. Haenggi, *Stochastic geometry for wireless networks*. Cambridge University Press, 2012.
[21] A. H. Sakr and E. Hossain, "Location-aware cross-tier coordinated multipoint transmission in two-tier cellular networks," *IEEE Trans. Wireless Commun.*, vol. 13, no. 11, pp. 6311–6325, Aug. 2014.
[22] H. A. David and H. N. Nagaraja, *Order statistics*. Wiley, 1970.
[23] I. S. Gradshteyn and I. M. Ryzhik, *Table of integrals, series, and products*. Academic press, 2014.

Yanan Liang (S'14) received the B.Sc. degree of Communication Engineering from Beijing Jiaotong University, China in 2013. She is currently working toward the Ph.D. degree of communication and information systems from Beijing Jiaotong University, China. From 2017 to 2018, she was a visiting Ph.D. student at the University of Notre Dame, Indiana, USA. Her research interests include random access schemes for 5G networks, machine-to-machine communications, and performance analysis of wireless self-organizing networks.

Xu Li (M'03) received the B.Sc. degree from Jilin University, China in 1991 and the Ph.D. degree from Northeastern University, China in 1997. Since 2003, she has been a Professor and Head of Wireless Self-Organizing Communications Group, School of Electronic and Information Engineering, Beijing Jiaotong University, China. She has published more than 60 papers and owns more than 40 patents. Her research interests include wireless self-organizing networks, wireless sensor networks and unmanned aerial vehicle systems.

Martin Haenggi (S'95-M'99-SM'04-F'14) received the Dipl.-Ing. (M.Sc.) and Dr.sc.techn. (Ph.D.) degrees in electrical engineering from the Swiss Federal Institute of Technology in Zurich (ETH) in 1995 and 1999, respectively. Currently he is the Freimann Professor of Electrical Engineering and a Concurrent Professor of Applied and Computational Mathematics and Statistics at the University of Notre Dame, Indiana, USA. In 2007-2008, he was a visiting professor at the University of California at San Diego, and in 2014-2015 he was an Invited Professor at EPFL, Switzerland. He is a co-author of the monographs "Interference in Large Wireless Networks" (NOW Publishers, 2009) and Stochastic Geometry Analysis of Cellular Networks (Cambridge University Press, 2018) and the author of the textbook "Stochastic Geometry for Wireless Networks" (Cambridge, 2012), and he published 15 single-author journal articles. His scientific interests lie in networking and wireless communications, with an emphasis on cellular, amorphous, ad hoc (including D2D and M2M), cognitive, and vehicular networks. He served as an Associate Editor of the Elsevier Journal of Ad Hoc Networks, the IEEE Transactions on Mobile Computing (TMC), the ACM Transactions on Sensor Networks, as a Guest Editor for the IEEE Journal on Selected Areas in Communications, the IEEE Transactions on Vehicular Technology, and the EURASIP Journal on Wireless Communications and Networking, as a Steering Committee member of the TMC, and as the Chair of the Executive Editorial Committee of the IEEE Transactions on Wireless Communications (TWC). From 2017 to 2018, he was the Editor-in-Chief of the TWC. He also served as a Distinguished Lecturer for the IEEE Circuits and Systems Society, as a TPC Co-chair of the Communication Theory Symposium of the 2012 IEEE International Conference on Communications (ICC'12), of the 2014 International Conference on Wireless Communications and Signal Processing (WCSP'14), and the 2016 International Symposium on Wireless Personal Multimedia Communications (WPMC'16). For both his M.Sc. and Ph.D. theses, he was awarded the ETH medal. He also received a CAREER award from the U.S. National Science Foundation in 2005 and three awards from the IEEE Communications Society, the 2010 Best Tutorial Paper award, the 2017 Stephen O. Rice Prize paper award, and the 2017 Best Survey paper award, and he is a 2017 and 2018 Clarivate Analytics Highly Cited Researcher.